

Accepted Manuscript

Research paper

Structure, spectra and electrical conductivity of Copper(I) and Silver(I) phosphino bridging mixed ligand complexes with Coumarinyl Schiff base

Suman Roy, Tapan Kumar Mondal, Animesh Layek, Rajat Saha, Chittaranjan Sinha

PII: S0020-1693(17)30266-9
DOI: <http://dx.doi.org/10.1016/j.ica.2017.08.031>
Reference: ICA 17825

To appear in: *Inorganica Chimica Acta*

Received Date: 22 February 2017
Revised Date: 3 July 2017
Accepted Date: 15 August 2017

Please cite this article as: S. Roy, T.K. Mondal, A. Layek, R. Saha, C. Sinha, Structure, spectra and electrical conductivity of Copper(I) and Silver(I) phosphino bridging mixed ligand complexes with Coumarinyl Schiff base, *Inorganica Chimica Acta* (2017), doi: <http://dx.doi.org/10.1016/j.ica.2017.08.031>

This is a PDF file of an unedited manuscript that has been accepted for publication. As a service to our customers we are providing this early version of the manuscript. The manuscript will undergo copyediting, typesetting, and review of the resulting proof before it is published in its final form. Please note that during the production process errors may be discovered which could affect the content, and all legal disclaimers that apply to the journal pertain.



**Structure, spectra and electrical conductivity of Copper(I) and Silver(I)
phosphino bridging mixed ligand complexes with Coumarinyl Schiff base**

Suman Roy^a, Tapan Kumar Mondal^a, Animesh Layek^b, Rajat Saha^b, and Chittaranjan Sinha^{*a}

^a Department of Chemistry, Inorganic Chemistry Section, Jadavpur University, Kolkata 700 032, India; ^b Department of Physics, Jadavpur University, Kolkata 700 032, India

ABSTRACT

Coordination polymers, $[-M(L)(\mu\text{-dppp/dppb/dpph})_n(X)]_n$, ($M = \text{Cu(I), Ag(I)}$; $L, N\text{-}\{(2\text{-pyridyl)methylidene}\}\text{-6-coumarin}$; $X = \text{NO}_3^-$ or ClO_4^- ; dppp, 1,3-bis(diphenylphosphino)propane; dppb, 1,4-bis(diphenylphosphino)butane; dpph, 1,6-bis(diphenylphosphino)hexane) have been spectroscopically characterised and one of the complexes, $[-\text{Ag(L)}(\mu\text{-dpph})_n(\text{NO}_3)_n]$ has been structurally supported by single crystal X-ray diffraction measurement. The current(I)-voltage(V) characteristics of the coordination polymer lies in the semiconductor range ($\sim 10^{-3} \text{ Sm}^{-1}$) and non-ohmic in nature; the band gap lies below 3.0 eV. The complexes are emissive in the visible region (509 – 522 nm) and solid phase emission is more intensive than solution phase. The cyclic voltammetry shows Cu(II)/Cu(I) couple at 0.8 – 0.9 V and ligand reductions at -0.59 to -0.69 V and -0.92 to -1.38 V. The spectral and conducting properties have been explained by DFT computation of molecular functions using optimised structures.

Keywords: Coumarinyl Schiff's base, Cu(I) and Ag(I) coordination polymer, X-ray structure, fluorescence, electrical conductivity

For Correspondence : c_r_sinha@yahoo.com

1. Introduction

The coordination polymers (CPs) of N, O-donor ligands are common [1, 2] while -S and -P donor centres have been poorly investigated [3,4]. Organophosphines (R_3P) are good candidates to alleviate lower oxidation states of the metal ions and the complexes are useful catalysts [5]. Bis(diphenylphosphino)alkane (alkane refers to propane or higher carbon system) constitutes coordination polymers [6,7] who have been used in different fields of science and engineering [8-10]. Metal-organic-coordination-polymers (MOCP) have widely used as conducting/semiconducting material [11] because of their accessible band gap (1.0 – 5.0 eV) [12].

Coumarinyl functionalised ligands have been used recently to design new molecules of varied interest [13]. Moreover, the Schiff bases of coumarin are useful fluorophores and laser dyes [14]. This has motivated us to synthesize N-[(2-pyridyl)methylidene]-6-coumarin (L) and to examine copper(I) and silver(I) complexes [15,16]. The field shell, d^{10} electronic configuration like Cu(I)-diimine has been extensively studied [17-22] while silver(I) complexes are relatively less documented [23]. It is reported that the metal complexes of d^{10} electronic configuration (Zn(II), Cu(I), Ag(I), Au(I) etc.) show metal centred (d-s, d- π) emission [24]. In this work, coordination polymers of Cu(I) and Ag(I) with L and bis(diphenylphosphino)alkane as bridging ligand, - $[-M(L)(\mu\text{-dppp})-]_n(X)_n$, $[-M(L)(\mu\text{-dppb})-]_n(X)_n$, $[-M(L)(\mu\text{-dpph})-]_n(X)_n$ ($M = \text{Cu(I), Ag(I)}$; $X = \text{NO}_3^-$ or ClO_4^-) have been reported. The structural elucidation is being done by spectroscopic data. The DFT computation of optimized structures have been used to determine electronic configuration which helps to explain the non-ohmic, current (I) – voltage (V) diagram and unusual electrical conductivity.

2. Results and discussion

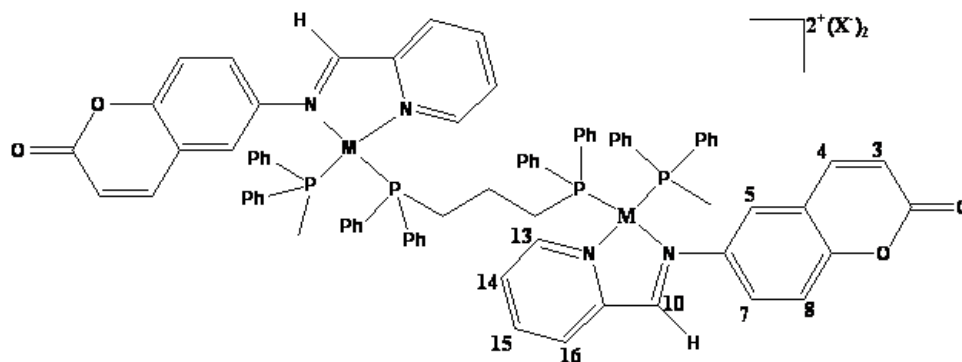
2.1. Synthesis and formulation

The reaction of L and dppp / dppb / dpph with $[\text{Cu}(\text{MeCN})_4]\text{ClO}_4$ (1: 1: 1 mole ratio) in dry methanol under N_2 environment has isolated $[-\text{Cu}(\text{L})(\mu\text{-dppp})-]_n(\text{ClO}_4)_n$ (**1**), $[-\text{Cu}(\text{L})(\mu\text{-dppb})-]_n(\text{ClO}_4)_n$ (**3**) and $[-\text{Cu}(\text{L})(\mu\text{-dpph})-]_n(\text{ClO}_4)_n$ (**5**) respectively (**Scheme 1**). The similar reaction using AgNO_3 or AgClO_4 under identical condition has separated $[-\text{Ag}(\text{L})(\mu\text{-dppp})-]_n(\text{X})_n$ (**2a**, **2b**), $[-\text{Ag}(\text{L})(\mu\text{-dppb})-]_n(\text{X})_n$ (**4a**, **4b**) and $[-\text{Ag}(\text{L})(\mu\text{-dpph})-]_n(\text{X})_n$ (**6a**, **6b**) [$\text{X} = \text{NO}_3^-$ (**a**) or ClO_4^- (**b**)] respectively (**Scheme 1**). The complexes are purified by crystallization through slow diffusion of hexane into dichloromethane solution of the complexes. The molar conductivity (Λ_M) of the complexes lie in the range $124 - 140 \Omega^{-1} \text{cm}^2 \text{mol}^{-1}$ (**1**, 129; **2a**, 126; **2b**, 129; **3**, 124; **4a**, 125; **4b**, 137; **5**, 130; **6a**, 140; **6b**, 137 $\Omega^{-1} \text{cm}^2 \text{mol}^{-1}$) which implies 1:1 electrolyte character considering the monomeric unit $[-\text{M}(\text{L})(\mu\text{-PPH}_2\text{-alkyl-PPH}_2)-]\text{X}$ ($\text{X} = \text{NO}_3^-$ or ClO_4^-). A solid state electrical conductivity measurement shows the semiconductive nature of the complexes (*vide infra*). The band gap of each material has been calculated with the help of Tauc's auxiliary equation [25].

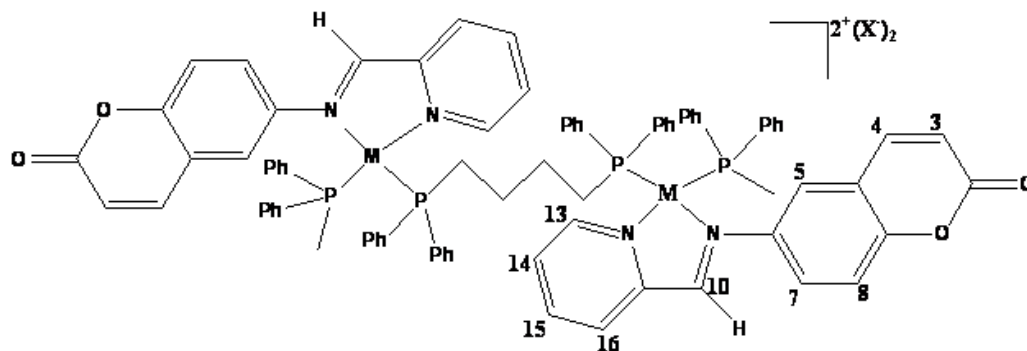
2.2. Molecular Structure of $[-\text{Ag}(\text{L})(\mu\text{-dpph})-]_n(\text{NO}_3)_n$ (**6a**)

$[-\text{Ag}(\text{L})(\mu\text{-dpph})-]_n(\text{NO}_3)_n$ (**6a**) crystallizes in *Monoclinic* crystal system of C2/c space group and the structure is shown in **Fig. 1**. The bond parameters are listed in **Table 1**. Ligand, L, acts as $\text{N,N}'$ -chelator (N refers to N(pyridyl) and N' refers to N(imine)) and dpph acts as bridging ligand to constitute coordination polymer (MOCP). The repeating unit $[-\text{Ag}(\text{L})(\mu\text{-dpph})-]$ is tetrahedral (**Fig. 1**) and the charges are satisfied by NO_3^- . The pendant coumarinyl ring makes a dihedral $38.70(19)^\circ$ with chelated diimine ring, $-(\text{Ag}-\text{N}=\text{C}-\text{C}=\text{N}-)$ and causes distortion from ideal platonic geometry. The chelate angle,

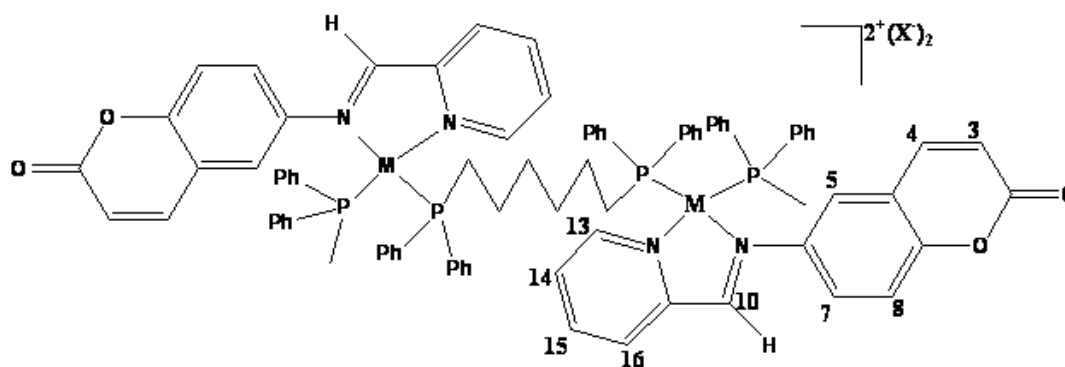
Ag(N, N'), 69.29(16)° is extended by L on coordination to Ag(I) and is comparable with reported results in the series of chelated diimine complexes of d¹⁰ metal ions [16]. The deviation from ideal tetrahedral ∠P(1)–Ag(1)–P(2) (123.26(5)°) supports the deviation from ideal geometry.



1 (M = Cu(I), X = ClO₄⁻), **2a** (M = Ag(I), X = NO₃⁻), **2b** (M = Ag(I), X = ClO₄⁻)



3 (M = Cu(I), X = ClO₄⁻), **4a** (M = Ag(I), X = NO₃⁻), **4b** (M = Ag(I), X = ClO₄⁻)



5 (M = Cu(I), X = ClO₄⁻), **6a** (M = Ag(I), X = NO₃⁻), **6b** (M = Ag(I), X = ClO₄⁻)

Scheme 1. The dimeric unit structure of the polymeric complexes

The deformation of the regular geometry may be due to steric requirement of pendant coumarinyl group of chelating unit and that of phenyl groups in -PPh₂. The Ag-N(pyridyl), 2.412(5) Å is longer than Ag(I)-N(imine), 2.384(4) Å, which reflects stronger interaction of Ag(I) with N(imine) compared to N(pyridyl) of L. The Ag-P distances, Ag(1)-P(1), 2.4170(15) and Ag(1)-P(2), 2.4768(16) Å have been deviated from [Ag(L)(PPh₃)₂][NO₃] [15] which may be due to steric demand of the coumarinyl part of the ligand. Each monomer is connected by C-H...O hydrogen bonding interactions to form supramolecular structure (**Fig. 2**). The interactions are C(2)-H(2)...O(2)(lactonyl) and C(8)-H(8)...O(5) (NO₃). The -PPh₂ phenyl hydrogen and nitrate-O interaction enhances the stability of the structure. Structural analysis shows the existence of cross π -interaction between coumarinyl Cg(2) : O(1), C(10), C(11), C(12), C(13), C(14) of one chain with Cg(4) : C(7), C(8), C(9), C(10), C(14), C(15) of adjacent chain (π -distance, Cg(2)...Cg(4), 3.720(3) Å; symmetry : 1-x, 1-y, 2-z). This is also contributing to improve structural stability.

2.3.1. The Spectral Characterization

In the infrared spectrum of the chelated L, the $\nu(\text{COO})$ appears at 1724 - 1735 cm^{-1} and that of $\nu(\text{C}=\text{N})$ appears at 1566-1568 cm^{-1} . These have been shifted from the free ligand ($\nu(\text{C}=\text{N})$, 1582 cm^{-1} and $\nu(\text{COO})$, 1714 cm^{-1}) data which confirms the binding of L to metal ion. The $\nu(\text{ClO}_4)$ appears at 1093-1097 cm^{-1} and a weak vibration at 623 cm^{-1} . In the complexes **2a**, **4a** and **6a** strong stretch at 1381, 1384 and 1382 cm^{-1} respectively refer to the presence of NO_3^- . The hydrogen bonded $-\text{ONO}_2^-$ in **6a** is confirmed by the doublet peak at 1382 and 1334 cm^{-1} (*vide* Experimental section).

Pyridyl protons (13-H to 16-H) experience significant downfield shift by 0.03-0.13 ppm while coumarinyl protons (3-H, 4-H, 5-H, 7-H, 8-H) are perturbed by 0.05-0.18 ppm. Imine proton ($-\text{CH}=\text{N}-$) appears as a singlet at 9.11 – 9.51 ppm. The proton movement is in association with coordination of L with metal ion(s). PPh_2 protons appear at 7.21 – 7.39 ppm. $\text{P}-(\text{CH}_2)_n-\text{P}$ ($n=3, 4, 6$) protons appear at 2.42-2.87(t), 1.91-2.69(m) and 1.31 – 1.35(s) (**5**, **6a** and **6b**) ppm (*vide* Experimental section). Similar signal movement suggests identical structure of the complexes.

2.3.2. Absorption and Emission spectra

The absorption bands at 330 – 340 nm are referred to intra-ligand or mixture of intra- and inter-ligand transitions of N-{(2-pyridyl)methylidene}-6-coumarin (L) [15] and phosphine (**Table 2, Fig. 3**). The low-energy absorptions at 400 – 455 nm of copper(I) complexes, **1**, **3** and **5**, are assigned to the admixture of metal-to-ligand ($\text{Cu}(d\pi) \rightarrow \text{L}(\pi^*)$) and inter-ligand (L and phosphine) charge transfer transitions [26-28]. Silver complexes (**2**, **4**, **6**) (*vide* Experimental section) do not show such bands which supports that copper(I) would be much more capable to assist MLCT transitions [29].

The ligand L exhibits emission at 484 nm at room temperature (298 K) upon excitation at 328 nm ($\pi-\pi^*$ state). $[-\text{Cu}(\text{L})(\mu\text{-dppp/dppb/dpph})-]_n(\text{X})_n$ complexes in the solid state and

in fluid solutions (**Fig. 4**) show intense long-lived orange emission upon excitation at 329-338 nm while Ag(I) complexes show weak green emission (**Fig. 5; Table 2**). The emission lifetimes in the nanosecond range suggest that the emissions are associated with a spin-forbidden transition (**Fig. 6, Table 2**). The emission energies of the complexes in solid state are lower than solution phase data. Possible assignments involve emissive states derived from ligand-centred IL ($\pi \rightarrow \pi^*$), metal-centred $d \rightarrow s$ or from either metal-to-ligand charge-transfer (MLCT) or ligand-to-metal charge-transfer (LMCT) transitions. Coumarinyl derivatives are important components of fluorescence probes, sensors, switches [30] and have been used for monitoring the polarity and micro-viscosity of the environment in various simple, mixed or ionic solvents [31] and were employed as reporter of radical reaction in the thin polymer films [32,33]. Substituted coumarin-like chromophores were used as molecular rotors and fluorescence probes for biological studies [34] as well. The complexes do not emit with sufficient intensity when they are excited at MLCT band maxima (>450 nm). Thus, the emission is originated from ligand centred excited states. The fluorescence quantum yield of the complexes are higher ($\phi = 0.046$ (**1**), 0.102 (**2a**), 0.089 (**2b**), 0.029 (**3**), 0.059 (**4a**), 0.045 (**4b**), 0.020 (**5**), 0.035 (**6a**) and 0.021 (**6b**)) than that of free ligand, L ($\phi = 0.018$). Increase in quantum yield of the complexes containing coordinated PPh_2 group may suggest structural distortion from a more planar in free ligand, L, to distorted structure. This is common in a tetrahedral geometry; besides, the presence of coordinated phosphine group will generate steric crowding to develop structural strain and may enhance steady state emissivity. In the series of three complexes $[-\text{M}(\text{L})(\mu\text{-dppp})\text{-}]_n(\text{X})_n$ (**1, 2a, 2b**), $[-\text{M}(\text{L})(\mu\text{-dppb})\text{-}]_n(\text{X})_n$ (**3, 4a, 4b**) and $[-\text{M}(\text{L})(\mu\text{-dpph})\text{-}]_n(\text{X})_n$ (**5, 6a, 6b**) [**1, 3, 5**: $\text{M} = \text{Cu}$, $\text{X} = \text{ClO}_4$; **2a, 4a, 6a**: $\text{M} = \text{Ag}$, $\text{X} = \text{NO}_3$; **2b, 4b, 6b**: $\text{M} = \text{Ag}$, $\text{X} = \text{ClO}_4$] ϕ follows the order **2a**>**2b**>**1**, **4a**>**4b**>**3**, **6a**>**6b**>**5** and **1**>**3**>**5**, **2a**>**4a**>**6a**, **2b**>**4b**>**6b**, respectively. Increase in alkyl chain length also reduces ϕ

which implies vibrational relaxation of excited state *via* alkyl chain [35]. Heteroatom containing fluorophores develop partial charges due to internal charge transfer (ICT) which can affect its energy [36]. In the complexes, the PET process is effectively decreased due to the presence of metal and π -acidic phosphine ligands which also helps to populate the excited states [37]. It may be one of the reasons for the increased fluorescence quantum yield of the complexes than ligand in presence of phosphine molecules. Copper(I) complexes show lower quantum efficiency than silver(I) analogues which may be due to photo-oxidation of copper(I) to copper(II) and the population of emitting species is thereby reduced [38]. The complexes are solution stable; even for a month solution does not change absorption characteristics. Besides, the solution is photostable and emission spectra remain unchanged for 30 min of light irradiation at 330 nm.

Solid state fluorescence of L and the complexes show emission at longer wavelength (λ_{em}) compared to solution phase emission (**Fig. 5, Table 2**) along with vibronic progression. In general, a tetrahedral coordination of Cu(I) complex in distorted geometry towards a square-planar in the excited state (flattening). Therefore, the reason for the difference between solid and solution phase is usually the difference in rigidity of the environment which influences the extent of flattening [39]. Besides, the restriction to vibrational relaxation in solid state relative to the solution phase may enhance the emissivity. The Cu(I) and Ag(I) are d^{10} electronic configuration in the complexes and they quench less retarding inter-system crossing (ISC) process *via* magnetic interaction [40, 41].

Life time data are obtained upon excitation at 370 nm and are summarized in **Table 2**. The fluorescence decay curve was deconvoluted with respect to the lamp profile. The observed fluorescence decay fits nicely with exponential decay profile for the complexes (**Fig. 6**) which is supported by goodness-of-fit (χ^2) data in the regression analyses. Radiative and

non-radiative rate constants (k_r and k_{nr}) show usual higher k_{nr} than k_r value. The excited state stability of $[-\text{Cu}(\text{L})(\mu\text{-dppp})]_n(\text{ClO}_4)_n$ (**1**), $[-\text{Ag}(\text{L})(\mu\text{-dppp})]_n(\text{X})_n$ (**2a**, **2b**), $[-\text{Ag}(\text{L})(\mu\text{-dppb})]_n(\text{X})_n$ (**4a**), $[-\text{Ag}(\text{L})(\mu\text{-dpph})]_n(\text{X})_n$ (**6a**) [$\text{X} = \text{NO}_3$ (**a**) or ClO_4 (**b**)] fit with single exponential decay curve whereas $[-\text{Cu}(\text{L})(\mu\text{-dppb})]_n(\text{ClO}_4)_n$ (**3**), $[-\text{Ag}(\text{L})(\mu\text{-dppb})]_n(\text{X})_n$ (**4b**), $[-\text{Cu}(\text{L})(\mu\text{-dpph})]_n(\text{ClO}_4)_n$ (**5**) and $[-\text{Ag}(\text{L})(\mu\text{-dpph})]_n(\text{X})_n$ (**6b**) fit with a bi-exponential decay curve which may be due to decay through both high energy and MLCT states. The average lifetime value for the complexes (Cu(I) complex, 7.44 – 9.28 ns; Ag(I) complex, 7.50 – 9.43 ns) is higher than free ligand data (0.92 ns) (**Table 2**). The metal-ligand orbital mixing in the complexes may be the reason for passing longer time at excited state. Previously examined Cu(I) complexes of L such as $[\text{Cu}(\text{L})_2]^+$, $[\text{CuX}(\text{L})(\text{PPh}_3)]$ ($\text{X} = \text{Cl}, \text{Br}, \text{I}$), $[\text{Cu}(\text{L})(\text{PPh}_3)_2]^+$ [15], $[(\text{L})\text{Cu}(\mu\text{-dppm})_2\text{Cu}(\text{L})](\text{ClO}_4)_2$, $[(\text{L})\text{Cu}(\text{CH}_3\text{CN})(\mu\text{-dppe})\text{Cu}(\text{CH}_3\text{CN})(\text{L})](\text{ClO}_4)_2$ [16], along with analogous Ag(I) complexes exhibit longer life excited states (**Fig. 7**). With increase in number of PPh_3 coordinated to Cu(I) the Stoke's shift ($\Delta\nu = \nu_{em} - \nu_a$) increases (**Fig. 8**) and their DFT calculation also show the increase in contribution of PPh_3 function to HOMO (**Fig. 9**). Although the emission is of $\pi\text{-}\pi^*$ origin but it has been significantly influenced by nature and electronic configuration of metal ion and ancillary ligands. The complexes in this work, $[-\text{M}(\text{L})(\mu\text{-bis}(\text{diphenylphosphino})\text{alkane})]_n^{n+}$, have similar coordination sphere; so the influence of ancillary coordinated ligand on the stability of $\pi\text{-}\pi^*$ level is more or less same which shows similar Stoke's shift as shown in **Fig. 8**.

The DFT computation of optimised geometry of two selective polymer forming motif of complex cation $[\text{Cu}(\text{L})(\mu\text{-dpph})]^+$ of **5** and $[\text{Ag}(\text{L})(\mu\text{-dpph})]^+$ of **6** have been used to assign the electronic transitions. The orbital energies along with contribution from the ligands and metal are given in *Supplementary Table (Tables S1 and S2 and Figures S1 and S2)* and

some selected MO's are given in **Fig. 10**. The HOMO-LUMO energy gap of monomeric unit, $[\text{Cu}(\text{L})(\mu\text{-dpph})]^+$ is 2.02 eV and that of $[\text{Ag}(\text{L})(\mu\text{-dpph})]^+$ is 1.84 eV. The bridging dpph mainly contributes to HOMO to HOMO-4 molecular functions while Cu(I) shares 39% of HOMO-5. In $[\text{Ag}(\text{L})(\mu\text{-dpph})]^+$ it is HOMO-6 who has 22% contribution from Ag(I). The ligand L contributes 97% to LUMO, LUMO+1 and LUMO+2 while LUMO+3 and higher energy unoccupied MOs carry 90-95% dpph character. Thus, electronic spectra may be considered as admixture of inter-ligand and MLCT transitions by participating levels of L, dpph and metal centre.

2.4. Electrochemistry and Electrical conductivity

In general Copper(I) complexes are electrochemically unstable unless stabilising force from ligand π -acidity encroach conjugation the metal-redox state. Diimine ($-\text{N}=\text{C}-\text{C}=\text{N}-$) and azoimine ($-\text{N}=\text{N}-\text{C}=\text{N}-$) functions form $[\text{Cu}(\text{N},\text{N})]^+$ chelating and stabilises Cu(I) centre. N- $\{(2\text{-Pyridyl})\text{methyliden}\}$ -6-coumarin belongs to $-\text{N}=\text{C}-\text{C}=\text{N}-$ and stabilizes $[\text{Cu}(\text{L})(\mu\text{-dpph})]^+$; besides dpph is also a low valent metal redox stabilizing agent. Copper(I) complexes show quasi-reversible oxidation-reduction Cu(II)/Cu(I) couple at *ca.* 0.8 – 0.9 V with reference to Ag/AgCl, Cl⁻ electrode and the quasi-reversible character is accounted from the ΔE_p ($E_{pa} - E_{pc}$) (130 – 150 mV) data; a small current is observed at 0.4 V which is considered for the oxidation of deposited copper on the electrode surface (Cu(I)/Cu(0)) (**Fig. 11, Table 2**). The $E_{\text{Cu(II)/Cu(I)}}$ appears at higher potential than that of reported voltage of $[\text{Cu}(\text{RaaiR}')_2]^+$ (RaaiR', 1-alkyl-2-(arylo)imidazoles) (0.4-0.5 V) [42]; $[\text{Cu}(\text{aap})_2]^+$ (0.6-0.7 V) (aap, 2-(arylo)pyridine) [43]; $[\text{Cu}(\text{aapm})_2]^+$ (aapm, 2-(arylo)pyrimidine) (0.65-0.75 V) [44]. This is to mention that $[\text{Cu}(\text{L})_2]^+$, $[\text{Cu}(\text{L})(\text{PPh}_3)_2]^+$ [15,16], $[\text{Cu}(\text{L})(\mu\text{-dppm})\text{Cu}(\text{L})]^{2+}$, $[\text{Cu}(\text{L})(\text{dppe})]^+$ [45] show Cu(II)/Cu(I) potential 0.7 – 0.9 V (L, N- $\{(2\text{-Pyridyl})\text{methyliden}\}$ -6-coumarin; dppm, bis(diphenylphosphino)methane (dppm), 1,2-bis(diphenylphosphino)

ethane (dppe)); presence of P-coordination in ternary complexes redox signal appears at higher voltage. The Cu(I) complexes in this work, $[-\text{Cu}(\text{L})(\mu\text{-dpph})\text{-}]_n(\text{ClO}_4)_n$, show even higher potential which may be in part from π -acidity of L and dppe and also from polymeric structure.

The cathodic progress followed by scan reversal in anodic side gives an irreversible oxidative response at 0.4 V which may be due to the oxidation of adsorbed silver on the electrode surface produced on the cathodic scan [25]. The reductive responses at -0.59 to -0.69 V and -0.92 to -1.38 V may be assigned to the reduction of diimine group of the chelated ligand. Free ligand does not show any oxidation but irreversible reductive response appear at < -1.5 V.

The complexes show electrical conductivity (**Fig. 12, Table 3**) and which are irrelevant with the thickness of the films. The conductivity data (**Table 3**) lie in the lower limit of semiconductor. The current-voltage diagram deviates from linearity and is non-ohmic which is the characteristics of the coordination polymers [46, 47]. The calculated band gap (< 3.0 eV) from UV-Vis spectral data (**Fig. 13**) supports the semi-conductivity nature. The conductivity follows the order $[-\text{M}(\mu\text{-dppe})\text{-}]_n^{n+} < [-\text{M}(\mu\text{-dppp})\text{-}]_n^{n+} < [-\text{M}(\mu\text{-dppb})\text{-}]_n^{n+}$ such as the data of Cu(I) complexes, $-\text{Cu}(\mu\text{-polyphosphino})\text{-}]_n(\text{ClO}_4)_n$ follow $1.95 \times 10^{-3} < 2.71 \times 10^{-3} < 4.38 \times 10^{-3} \text{ S m}^{-1}$ and data of $-\text{Ag}(\mu\text{-polyphosphino})\text{-}]_n(\text{ClO}_4)_n$ follow $1.46 \times 10^{-3} < 2.92 \times 10^{-3} < 4.35 \times 10^{-3} \text{ S m}^{-1}$ (**Table 3**). The conductivity data are very low and data have not been affected by film length and thickness. The chain length of μ -polyphosphino bridge may be the reason for change of conductivity [48]. The co-ordination polymers in presence of counter ion ClO_4^- show higher conductivity in comparison to the polymers with counter ion NO_3^- , which is also supported by the measured energy band gap. Four oxygen units in ClO_4^- compared to three O-centres in NO_3^- may improve substantially the hydrogen bonding

strength in the former complex which may provide higher rigidity in the solid state geometry and hence favours the conductivity [49]. Besides, the π --- π interactions (between coumarin aromatics) may be responsible for electron delocalization in molecular conductors as those of the thionate family [48].

3. Conclusion

Mixed ligand Cu(I) and Ag(I) complexes of 1,3-bis(diphenylphosphino)propane (dppp) / 1,4-bis(diphenylphosphino)butane (dppb) / 1,6-bis(diphenylphosphino)hexane (dpph) and N-{(2-pyridyl)methylidene}-6-coumarin (L) constitute a member of metal-organic coordination polymer. The complexes show high intense emission compared to free L. The electrical conductivity of the coordination polymers shows semiconductivity ($\sim 10^{-3} \text{ Sm}^{-1}$) and the band gap lies $< 3.0 \text{ eV}$. This work has motivated us to design different classes of coumarinyl derivatives for improving semiconductive activity of MOCPs.

4. Experimental

4.1. Materials and physico-chemical techniques

AgNO_3 , $\text{AgClO}_4 \cdot x\text{H}_2\text{O}$, 1,3-bis(diphenylphosphino)propane (dppp), 1,4-bis(diphenylphosphino)butane (dppb), 1,6-bis(diphenylphosphino)hexane (dpph) and pyridine-2-carboxaldehyde were purchased from Aldrich Chemical Co. Coumarin was available from S. D. Fine Chem. Ltd., Boisar. N-{(2-pyridyl)methylidene}-6-coumarin (L) was synthesised following the reported procedure [15]. $[\text{Cu}(\text{MeCN})_4]\text{ClO}_4$ was prepared by standard procedure [26]. All the solvents were dried and purified by standard methods [44]. The acetonitrile used for electrochemical studies was dried with CaH_2 and distilled prior to use [50]. Dinitrogen was purified by bubbling through an alkaline pyrogallol solution. All other chemicals were of reagent grade and were used without further purification.

Microanalytical data (C, H, N) were collected on Perkin-Elmer 2400 CHNS/O elemental analyzer. Spectroscopic data were obtained using the following instruments: UV-Vis spectra by Perkin Elmer UV-Vis spectrophotometer model Lambda 25; FTIR spectra (KBr disk, 4000-400 cm^{-1}) by Perkin Elmer FT-IR spectrophotometer model RX-1; the ^1H NMR spectra by Bruker (AC) 300 MHz FTNMR spectrometer. Emission was examined by LS 55 Perkin Elmer spectrofluorimeter at room temperature (298 K) in CH_3CN solution under degassed condition. Electrochemical measurements were performed using computer-controlled CH-Instruments, Electrochemical workstation, Model No CHI 600D (SPL) with Pt-disk electrodes. All measurements were carried out under nitrogen environment at 298 K with reference to Ag/AgCl electrode in acetonitrile and dimethylformamide using $[\text{nBu}_4\text{N}]\text{ClO}_4$ as supporting electrolyte.

The fluorescence quantum yield of the complexes was determined using carbazole as a reference with known ϕ_R of 0.42 in benzene [51]. The complex and the reference dye were excited at same wavelength, maintaining nearly equal absorbance (~ 0.1), and the emission spectra were recorded. The area of the emission spectrum was integrated using the software available in the instrument and the quantum yield is calculated according to the following Eq. (1) :

$$\phi_S/\phi_R = [A_S / A_R] \times [(Abs)_R / (Abs)_S] \times [\eta_S^2/\eta_R^2] \quad (1)$$

Here, ϕ_S and ϕ_R are the fluorescence quantum yield of the sample and reference, respectively. A_S and A_R are the area under the fluorescence spectra of the sample and the reference respectively, $(Abs)_S$ and $(Abs)_R$ are the respective optical densities of the sample and the reference solution at the wavelength of excitation, and η_S and η_R are the values of refractive index for the respective solvent used for the sample and reference.

Fluorescence lifetimes were measured using a time-resolved spectrofluorimeter from IBH, UK. The instrument uses a picoseconds diode laser (NanoLed-07, 370 nm) as the excitation source and works on the principle of time-correlated single photon counting [52]. The instrument responses function is ~ 230 ps at FWHM. To eliminate depolarization effects on the fluorescence decays, measurements were done with magic angle geometry (54.7°) for the excitation and emission polarizers. The observed decays of **1**; **2a**, **2b**; **4a**; **6a** fit with single exponential decay whereas **3**, **4b**, **5** and **6b** fit with a bi-exponential decay as in the following equation (Eqs. (2) and (3)), where τ 's are the fluorescence lifetime and α is the pre-exponential factor. For the fits, the reduced χ^2 values were within 0.98 – 1.25 and the distribution of the weighted residuals were random among the data channels. τ_f is mean fluorescence life time (meaning of the symbols are usual) [53].

$$I(t) = [a_1 \exp(-t / \tau_1) - a_2 \exp(-t / \tau_2)] \quad (2)$$

$$\tau_f = a_1 \tau_1 + a_2 \tau_2 \quad (3)$$

Electric conductivity of a material is a measure of its ability to conduct electric current or free charge carriers under certain conditions such as temperature, pressure, applied voltage etc. In case of ohmic conducting materials the conductivity mainly depends on the effective resistance of the materials. To measure the conducting property of any substance, resistance of the substance is to be calculated by applying certain voltage across a specific dimension and measuring corresponding current. It is quite straight forward that by applying Ohm's law resistivity as well as conductivity can be measured by optimizing the dimension of the materials. In this study, we have deposited a thin film of given sample which is well dispersed in dichloromethane. At first the sample was mixed with the solvent and was sonicated for about 30 minutes until the sample was well dispersed. A glass substrate was

cleaned by acetone, ethanol and distilled water accordingly with ultra-sonicator and was dried. On to the cleaned glass substrate, dispersed solution was spin coated at 1200 rpm for 2 minutes. As the thin film achieved the thickness of the film was measured, after drying the film at about 80°C inside a vacuum oven, as 400 nm by surface profiler. Then aluminium electrodes were deposited on to the thin film through masking by Vacuum Coating Unit 12A4D of HINDHIVAC under low pressure 10⁻⁶ milli barr. The dimension of the aluminium strips are of 9 mm X 1 mm with a gapping of 1.5 mm between two electrodes (*Supplementary Materials, Fig. S3*). The masks were adjusted in such a way that the dimension of the effective film maintained 9 mm X 1.5 mm effective area. Afterward the electrodes were connected with a KEITHLEY 2400 source meter by two-probe contact to measure the conductivity by using applied Voltage-Current profiles. All these procedure had been performed under room temperature and atmospheric pressure. Using the slope of I-V characteristic curve and considering the dimension of the film (effective length, l ; cross section, $a \times d$) conductivity can be measured with the help of equation (Eq. (4)) as mentioned below.

$$\text{Conductivity } (\sigma) = (\text{slope}) \times \{l/(a \times d)\} \quad (4)$$

In this work the data are : effective length (l) = 1.5x10⁻¹ cm, cross section [(A) = $a \times d$] = 36 x10⁻⁶ cm², * σ = slope x (l/A)

The solid state absorption of the co-ordination polymer thin film indicates the sharp excitation wavelength, signifies every possibility of charge transportation under imposing of external constraints. Hence it is important to evaluate the significant energy gap. The band gap of mixed ligand co-ordination polymer arises due to the formation of localized states, which are trapped near the band edges of the materials. These localized states are responsible for transportation of charge carriers, which also improve the conductivity by reducing the

active impedance. The band gap of these polymer grade materials were measured by using the Tauc's equation with the help of absorption spectra. Tauc [54] showed that the shape and position of the absorption edge for high absorption region could be represented by the equation (Eq. (5))

$$\alpha(\omega) = A(\hbar\omega - E_g)^{1/2} / \hbar\omega \quad (5)$$

where α is absorption co-efficient for non-direct transition, ω is angular frequency, A is a constant and E_g is the optical energy gap. To determine the absorption coefficient the following equation (Eq. (6)) was used,

$$\alpha(\omega) = (1/d) \ln(1/T_r) \quad (6)$$

where, T_r is the transmittance and d is the sample thickness. By measuring the intercept on incident (photon) energy axis in $(\alpha h\nu)^2$ vs $h\nu$ plot, with the help of UV-VIS absorption data, the value of E_g for each samples were evaluated (**Table 3**).

4.2. Syntheses of [-Cu(L)(μ -dppp)-]_n (ClO₄)_n (1)

[Cu(MeCN)₄]ClO₄ (0.025 g, 0.076 mmol) was taken in a double neck Round Bottom flask dissolved in dry MeOH by magnetic stirring under N₂ atmosphere. Then 1,3-bis(diphenylphosphino)propane (dppp) (0.0314 g, 0.076 mmol) was added to this solution and stirred magnetically. After half an hour L (0.019 g, 0.076 mmol) was added to the reaction mixture and stirred for another two hours. The solution colour turned to red. It was filtered and kept undisturbed for crystallisation. The complex was obtained in 0.047 g (75%) yield; decomposition temperature > 120°C. MS m/z = 725.6 ([Cu(L)(dppp)]⁺), 475.5 ([Cu(dppp)]⁺) (**Supplementary Material, Fig. S4**); ¹H NMR (300 MHz, CDCl₃) δ 2.48(t), 2.69 (m) (P-(CH₂)₃-P), 6.61 (1H, d, 9.6 Hz, 3-H), 7.23 (1H, d, 7.9 Hz, 7-H), 7.21-7.35 (m) (-

PPh₂), 7.48 (1H, s, 5-H), 7.51 (1H, d, 7.5 Hz, 8-H), 7.52 (1H, d, 8.6 Hz, 4-H), 7.62 (1H, t, 7.8 Hz, 14-H), 7.92 (1H, m, 15-H), 8.63 (1H, d, 6.8 Hz, 16-H), 8.71 (1H, d, 6.9 Hz, 13-H). FT-IR(KBr, ν cm⁻¹) ν (COO), 1728; ν (C=N), 1567; ν (ClO₄) 1094 (s), 622 (w); UV (λ_{\max} , nm (ϵ , 10³M⁻¹ cm⁻¹) in CH₃CN), 454(0.97), 338(8.2), 275(28.8); C₄₂H₃₆ClCuN₂O₆P₂: Anal. Found: C, 61.23; H, 4.42; N, 3.30 ; Calc.: C, 61.09; H, 4.36; N, 3.39%.

[-Cu(L)(μ -dppb)-]_n (ClO₄)_n (3) and [-Cu(L)(μ -dpph)-]_n (ClO₄)_n (5)

Both the complexes were synthesized using the same procedure mentioned above for [-Cu(L)(μ -dppp)-]_n(ClO₄)_n (1) taking the reactants in equi molar ratio and in each case the solution turned to red.

[-Cu(L)(μ -dppb)-]_n (ClO₄)_n (3): The complex was obtained in 0.045 g (70%) yield; decomposition temperature > 140°C. MS m/z = 739.7 ([Cu(L)(bppb)]⁺), 489.6 ([Cu(bppb)]⁺) (Supplementary Material, Fig. S5); ¹H NMR (300 MHz, CDCl₃) δ 2.42 (t), 2.63 (m) (P-(CH₂)₄-P), 6.57 (1H, d, 9.6 Hz, 3-H), 7.12 (1H, d, 7.8 Hz, 7-H), 7.21-7.35 (m) (-PPh₂), 7.34 (1H, s, 5-H), 7.39 (1H, d, 7.3 Hz, 8-H), 7.47 (1H, d, 8.4 Hz, 4-H), 7.49 (1H, t, 7.8 Hz, 14-H), 7.89 (1H, m, 15-H), 8.23 (1H, d, 6.6 Hz, 16-H), 8.54 (1H, d, 6.8 Hz, 13-H). FT-IR(KBr, ν cm⁻¹) ν (COO), 1735; ν (C=N), 1566; ν (ClO₄) 1094 (s), 623 (w); UV (λ_{\max} , nm (ϵ , 10³M⁻¹ cm⁻¹) in CH₃CN), 406(2.0), 333(11.6), 278 (34.2); C₄₃H₃₈ClCuN₂O₆P₂: Anal. Found: C, 61.40; H, 4.40; N, 3.44 ; Calc.: C, 61.53; H, 4.53; N, 3.34%.

[-Cu(L)(μ -dpph)-]_n (ClO₄)_n (5): The complex was obtained in 0.053 g (80%) yield; decomposition temperature > 160°C. MS m/z = 767.5 ([Cu(L)(dpph)]⁺), 517.5 ([Cu(dpph)]⁺); ¹H NMR (300 MHz, CDCl₃) δ 1.31 (s), 2.87 (t) (P-(CH₂)₆-P), 6.53 (1H, d, 9.4 Hz, 3-H), 7.05 (1H, d, 7.6 Hz, 7-H), 7.25-7.38 (m) (-PPh₂), 7.24 (1H, s, 5-H), 7.32 (1H, d, 7.3 Hz, 8-H), 7.43 (1H, d, 8.3 Hz, 4-H), 7.46 (1H, t, 7.8 Hz, 14-H), 7.89 (1H, m, 14-H), 8.13 (1H, d, 6.6 Hz, 16-

H), 8.37 (1H, d, 6.8 Hz, 13-H); FT-IR(KBr, ν cm^{-1}) $\nu(\text{COO})$, 1728; $\nu(\text{C}=\text{N})$, 1566; $\nu(\text{ClO}_4)$ 1093 (s), 623 (w); UV (λ_{max} , nm (ϵ , $10^3\text{M}^{-1}\text{cm}^{-1}$) in CH_3CN), 427(1.9), 330(12.1), 270(39.9); $\text{C}_{45}\text{H}_{42}\text{ClCuN}_2\text{O}_6\text{P}_2$: Anal. Found: C, 62.37; H, 4.77; N, 3.19; Calc.: C, 62.28; H, 4.84; N, 3.23%.

$[-\text{Ag}(\text{L})(\mu\text{-dppp})\text{-}]_n(\text{NO}_3)_n$ (2a)

To AgNO_3 (0.025 g, 0.15 mmol) solution in MeOH (20 ml) in dark and stirring condition, 1,3-bis(diphenylphosphino)propane (dppp) (0.0605 g, 0.15 mmol) was added and stirred for one hour. Then L (0.0368 g, 0.15 mmol) was added to this solution and was magnetically stirred for two hours. Light yellow solution was obtained. It was filtered and kept undisturbed for crystallisation. The complex was obtained in 0.092 g (75%) yield; decomposition temperature $>153^\circ\text{C}$. MS $m/z = 770.0$ ($[\text{Ag}(\text{L})(\text{dppp})]^+$), 520.0 ($[\text{Ag}(\text{dppp})]^+$); ^1H NMR (300 MHz, CDCl_3) δ 2.42(t), 2.63(m) P-(CH_2)₃-P, 6.57(1H, d, 9.5 Hz, 3-H), 7.19 (1H, d, 7.8 Hz, 7-H), 7.23-7.37 (-PPh₂), 7.43 (1H, s, 5-H), 7.47(1H, d, 8.5 Hz, 4-H), 7.48 (1H, d, 7.4 Hz, 8-H), 7.55 (1H, m, 14-H), 7.85 (1H, m, 15-H), 8.61(1H, d, 6.6 Hz, 16-H), 8.65 (1H, d, 6.7 Hz, 13-H), 9.46 (1H, s, 10-H), FT-IR(KBr, ν cm^{-1}) $\nu(\text{COO})$, 1724; $\nu(\text{C}=\text{N})$, 1567; $\nu(\text{NO}_3)$ 1381, 1339; UV (λ_{max} , nm (ϵ , $10^3\text{M}^{-1}\text{cm}^{-1}$) in CH_3CN), 336(7.0), 273 (31.5), 243 (35.1); $\text{C}_{42}\text{H}_{36}\text{AgN}_3\text{O}_5\text{P}_2$: Anal. Found: C, 60.50; H, 4.31; N, 4.98; Calc.: C, 60.58; H, 4.33; N, 5.05%.

$[-\text{Ag}(\text{L})(\mu\text{-dppb})\text{-}]_n(\text{NO}_3)_n$ (4a) and $[-\text{Ag}(\text{L})(\mu\text{-dpph})\text{-}]_n(\text{NO}_3)_n$ (6a)

Both the complexes were synthesized using the same procedure mentioned above for $[-\text{Ag}(\text{L})(\mu\text{-dppp})\text{Ag}(\text{L})\text{-}]_n(\text{NO}_3)_{2n}$ (2a) taking the reactants in equi molar ratio and in each case the solution turned to yellow.

$[-\text{Ag}(\text{L})(\mu\text{-dppb})\text{-}]_n(\text{NO}_3)_n$ (**4a**): The complex was obtained in 0.087 g (70%) yield; decomposition temperature $> 160^\circ\text{C}$. MS $m/z = 784.0$ ($[\text{Ag}(\text{L})(\text{bppb})]^+$), 534.0 ($[\text{Ag}(\text{bppb})]^+$); ^1H NMR (300 MHz, CDCl_3) δ 1.91 (m), 2.65 (t), P-(CH_2)₄-P, 6.53 (1H, d, 9.4 Hz, 3-H), 7.21-7.37 -PPh₂, 7.11 (1H, d, 7.7 Hz, 7-H), 7.31 (1H, s, 5-H), 7.36 (1H, d, 7.2 Hz, 8-H), 7.43 (1H, d, 8.2 Hz, 4-H), 7.43 (1H, m, 14-H), 7.87 (1H, m, 15-H), 8.21 (1H, d, 6.5 Hz, 16-H), 8.51 (1H, d, 6.6 Hz, 13-H), 9.11 (1H, s, 10-H), FT-IR(KBr, ν cm^{-1}) $\nu(\text{COO})$, 1724; $\nu(\text{C}=\text{N})$, 1563; $\nu(\text{NO}_3)$ 1384; UV (λ_{max} , nm (ϵ , $10^3\text{M}^{-1}\text{cm}^{-1}$) in CH_3CN), 329 (28.8), 278 (68.2), 249 (52.9); $\text{C}_{43}\text{H}_{38}\text{AgN}_3\text{O}_5\text{P}_2$: Anal. Found: C, 60.90; H, 4.57; N, 5.00; Calc.: C, 60.99; H, 4.49; N, 4.96%.

$[-\text{Ag}(\text{L})(\mu\text{-dpph})\text{-}]_n(\text{NO}_3)_n$ (**6a**): The complex was obtained in 0.103 g (80%) yield; decomposition temperature $> 180^\circ\text{C}$. MS $m/z = 812.0$ ($[\text{Ag}(\text{L})(\text{dpph})]^+$), 562.0 ($[\text{Ag}(\text{dpph})]^+$); ^1H NMR (300 MHz, CDCl_3) δ 1.33(s), 2.83(t), P-(CH_2)₆-P, 6.51 (1H, d, 9.3 Hz, 3-H), 7.03 (1H, d, 7.5 Hz, 7-H), 7.22 (1H, s, 5-H), 7.27-7.39 -PPh₂, 7.31 (1H, d, 7.2 Hz, 8-H), 7.41 (1H, d, 8.2 Hz, 4-H), 7.41 (1H, m, 14-H), 7.83 (1H, m, 15-H), 8.35 (1H, d, 6.6 Hz, 13-H), 8.11 (1H, d, 6.5 Hz, 16-H), 9.09 (1H, s, 10-H), FT-IR(KBr, ν cm^{-1}) $\nu(\text{COO})$, 1730; $\nu(\text{C}=\text{N})$, 1568; $\nu(\text{NO}_3)$ 1382, 1334; UV (λ_{max} , nm (ϵ , $10^3\text{M}^{-1}\text{cm}^{-1}$) in CH_3CN), 334 (9.4), 279 (24.5), 246 (38.4); $\text{C}_{45}\text{H}_{42}\text{AgN}_3\text{O}_5\text{P}_2$: Anal. Found: C, 61.66; H, 4.89; N, 4.70; Calc.: C, 61.78; H, 4.81; N, 4.81%.

$[-\text{Ag}(\text{L})(\mu\text{-dppp})\text{-}]_n(\text{ClO}_4)_n$ (**2b**), $[-\text{Ag}(\text{L})(\mu\text{-dppb})\text{-}]_n(\text{ClO}_4)_n$ (**4b**) and $[-\text{Ag}(\text{L})(\mu\text{-dpph})\text{-}]_n(\text{ClO}_4)_n$ (**6b**)

The syntheses of all these three complexes were done following the same procedure of the above three silver complexes (**2a**, **4a**, and **6a**) except that AgClO_4 was taken in place of AgNO_3 in equi molar ratio with ligand and in each case the solution turned to yellow. In case

of **6a** the yellow complex obtained after evaporating the CH₃OH solution was dissolved in CH₂Cl₂ and layered by hexane to get single crystal. No such single crystal was obtained in case of other silver complexes.

[-Ag(L)(μ-dppp)-]_n(ClO₄)_n (**2b**): The complex was obtained in 0.073 g (70%) yield; decomposition temperature >130°C. MS m/z = 770.0 ([Ag(L)(dppp)]⁺), 520.0 ([Ag(dppp)]⁺); ¹H NMR (300 MHz, CDCl₃) δ 2.46(t), 2.67(m) P-(CH₂)₃-P, 6.59 (1H, d, 9.6 Hz, 3-H), 7.21-7.35 -PPh₂, 7.23 (1H, d, 7.9 Hz, 7-H), 7.47 (1H, s, 5-H), 7.51 (1H, d, 8.6 Hz, 4-H), 7.52 (1H, d, 7.5 Hz, 8-H), 7.62 (1H, m, 14-H), 7.91 (1H, m, 15-H), 8.63(1H, d, 6.7 Hz, 16-H), 8.67(1H, d, 6.8 Hz, 13-H), 9.49 (1H, s, 10-H); FT-IR(KBr, ν cm⁻¹) ν(COO), 1727; ν(C=N), 1568; ν(ClO₄) 1095 (s), 622 (w); UV (λ_{max}, nm (ε, 10³M⁻¹ cm⁻¹) in CH₃CN), 332 (11.9), 273 (44.4), 247 (38.1); C₄₂H₃₆ClAgN₂O₆P₂: Anal. Found: C, 57.92; H, 4.20; N, 3.14 Calc.: C, 57.96; H, 4.14; N, 3.22%.

[-Ag(L)(μ-dppb)-]_n(ClO₄)_n (**4b**): The complex was obtained in 0.080 g (75%) yield; decomposition temperature > 190°C. MS m/z = 784.0 ([Ag(L)(bppb)]⁺), 534.0 ([Ag(bppb)]⁺); ¹H NMR (300 MHz, CDCl₃) δ 1.95(m), 2.67(t), P-(CH₂)₄-P, 6.56 (1H, d, 9.5 Hz, 3-H), 7.23-7.39 -PPh₂, 7.15 (1H, d, 7.8 Hz, 7-H), 7.35 (1H, s, 5-H), 7.39 (1H, d, 7.3 Hz, 8-H), 9.13(1H, s, 10-H), 7.47(1H, d, 8.4 Hz, 4-H), 7.68 (1H, m, 14-H), 7.97 (1H, m, 15-H), 8.23 (1H, d, 6.6 Hz, 16-H), 8.54 (1H, d, 6.8 Hz, 13-H); 9.13 (1H, s, 10-H); FT-IR(KBr, ν cm⁻¹) ν(COO), 1728; ν(C=N), 1566; ν(ClO₄) 1094 (s), 622 (w); UV (λ_{max}, nm (ε, 10³M⁻¹ cm⁻¹) in CH₃CN), 333 (12.8), 275 (38.4), 244 (44.7); C₄₃H₃₈ClAgN₂O₆P₂: Anal. Found: C, 58.31; H, 4.34; N, 3.26; Calc.: C, 58.40; H, 4.30; N, 3.17%.

[-Ag(L)(μ-dpph)-]_n(ClO₄)_n (**6b**): The complex was obtained in 0.088 g (80%) yield; decomposition temperature > 160°C. MS m/z = 812.0([Ag(L)(dpph)]⁺), 562.0([Ag(dpph)]⁺);

^1H NMR (300 MHz, CDCl_3) δ 1.35(s), 2.85(t), P-(CH_2)₆-P, 6.53 (1H, d, 9.4 Hz, 3-H), 7.25-7.37 -PPh₂, 7.07 (1H, d, 7.6 Hz, 7-H), 7.23(1H, s, 5-H), 7.35 (1H, d, 7.4 Hz, 8-H), 7.43(1H, d, 8.4 Hz, 4-H), 7.43 (1H, m, 14-H), 7.87 (1H, m, 15-H), 8.15 (1H, d, 6.6 Hz, 16-H), 8.37 (1H, d, 6.7 Hz, 13-H), 9.11 (1H, s, 10-H); FT-IR(KBr, ν cm^{-1}) $\nu(\text{COO})$, 1726; $\nu(\text{C}=\text{N})$, 1567; $\nu(\text{ClO}_4)$ 1097 (s), 623 (w); UV (λ_{max} , nm (ϵ , $10^3\text{M}^{-1}\text{cm}^{-1}$) in CH_3CN), 333 (7.0), 274 (23.0), 246 (37.5); $\text{C}_{45}\text{H}_{42}\text{ClAgN}_2\text{O}_6\text{P}_2$: Anal. Found: C, 59.11; H, 4.68; N, 3.12 ; Calc.: C, 59.24; H, 4.61; N, 3.07%.

4.3. X-ray Crystallography of [-Ag(L)(μ -dpph)-]_n(NO₃)_n (**6a**)

The crystal was obtained by slow evaporation of acetonitrile solution of [-Ag(L)(μ -dpph)-]_n(NO₃)_n (**6a**) (0.22×0.14×0.10 mm). Data for **6a** was collected by Bruker Smart CCD Area Detector at 293(2) K. Diffractions were recorded with 2θ in the range $2.64 \leq 2\theta \leq 52.28$. Fine-focus sealed tube was used as the radiation source of graphite-monochromatized MoK α radiation ($\lambda = 0.71073$ Å). Multiscan absorption correction in the $h k l$ range: $-15 \leq h \leq 15$; $-27 \leq k \leq 27$; $-38 \leq l \leq 38$. Multiscan absorption correction was accomplished with the program SADABS [55]. Crystallographic refinement data and selected geometric parameters are collected in **Table 4**. Full matrix least squares refinements on F^2 were carried out using SHELXL-97 with anisotropic displacement parameters for all non-hydrogen atoms [56, 57]. Hydrogen atoms were constrained to ride on the respective carbon atoms with isotropic displacement parameters equal to 1.2 times the equivalent isotropic displacement of their parent atom in all cases of aromatic units. The figures were drawn with PLATON for [-Ag(L)(μ -dpph)-]_n(NO₃)_n (**6a**) [58].

4.4. Theoretical Calculations

The energy calculation and orbital picture of the complexes (**5**, **6**) were carried out using density functional theory (DFT) at the B3LYP level considering the crystal structure as the optimised structure and taking the unit $[M(L)(dpph)_2]^+$ since we are unable to optimise taking the whole polymer [59]. All calculations were carried out using the Gaussian 03 program package [60] with the aid of the GaussView visualization program [61]. For C, H, N, O and P the 6-31G (d), while for Cu, LANL2DZ and for Ag SDD basis set with effective core potential was employed [62]. Gauss Sum was used to calculate the fractional contributions of various groups to each molecular orbital [63].

Supporting Information

Crystallographic data for the structures have been deposited to the Cambridge Crystallographic Data center, CCDC 934242, $[-Ag(L)(\mu-dpph)-]_n(NO_3)_n$ contain the supplementary crystallographic data. These data can be obtained free of charge via <http://www.ccdc.cam.ac.uk/conts/retrieving.html>, or from the Cambridge Crystallographic Data Centre, 12 Union Road, Cambridge CB2 1EZ, UK; fax: (+44) 1223-336-033; or e-mail: deposit@ccdc.cam.ac.uk.

Acknowledgements

Financial support from the Council of Scientific and Industrial Research (01(2731)/13/EMR-II) and University Grants Commission (F. 42-333/2013(SR)), New Delhi are thankfully acknowledged.

References

- [1] M. Fujita, M. Tominaga, A. Hori, B. Therrien, *Acc. Chem. Res.* 38 (2005) 369–378.
- [2] S. Hiraoka, K. Harano, M. Shiro, M. Shionoya, *Angew. Chem., Int. Ed.* 44 (2005) 2727-2731.
- [3] J. L. C. Rowsell, O. M. Yaghi, *Microporous Mesoporous Mater.* 73 (2004) 3-14.
- [4] M. J. Rosseinsky, *Microporous Mesoporous Mater.* 73 (2004) 15-30.
- [5] L. H. Pignolet, *Homogeneous Catalysis with Metal Phosphine Complexes*; Plenum: New York (1983).
- [6] P. W. Miller, M. Nieuwenhuyzen, J. P. H. Charmant, S. L. James, *Inorg. Chem.*, 47 (2008) 8367-8379.
- [7] P. M. Van Calcar, M. M. Olmstead, A. L. Balch, *Inorg. Chem.* 36 (1997) 5231-5238.
- [8] K. Fromm, *Coord. Chem. Rev.* 252 (2008) 856–885.
- [9] X. You, *Coord. Chem. Rev.* 359 (2006) 3257–3263.
- [10] A. U. Czaja, N. Trukhan, U. Muller, *Chem. Soc. Rev.* 38 (2009) 1284–1293.

- [11] W R Salaneck, D T Clark, E J Samuelsen, *Science and Applications of Conducting Polymers*, Published by Adam Hilger, Bristol (1991).
- [12] G. Givaja, P. Ami-Ochoa, C. J. Gomez-Garcia, F. Zamora, *Chem. Soc. Rev.* 41 (2012) 115-147.
- [13] R. Murray, J. Mendez, S. Brown, *The Natural Coumarins: Occurrence, Chemistry, and Biochemistry*, Wiley, New York (1982).
- [14] O. D. Kachkovski, O. I. Tolmachev, L. O. Kobryn, E. E. Bila, M. I. Ganushchak, *Dyes Pigments* 63 (2004) 203–211.
- [15] S. Roy, T. K. Mondal, P. Mitra, E. L. Torres, C. Sinha, *Polyhedron* 30 (2011) 913-922.
- [16] S. Roy, T. K. Mondal, P. Mitra, C. Sinha, *Polyhedron* 51 (2013) 27-40.
- [17] D. R. McMillin, J. R. Kirchhoff, K. V. Goodwin, *Coord. Chem. Rev.* 64 (1985) 83-92.
- [18] D. R. McMillin, F. Liu, K. A. Meadows, T. K. Aldridge, B. P. Hudson, *Coord. Chem. Rev.* 132 (1994) 105-112.
- [19] M. T. Miller, P. K. Gantzel, T. B. Karpishin, *Inorg. Chem.* 38 (1999) 3414-3422.
- [20] M. K. Eggleston, D. R. McMillin, K. S. Koenig, A. J. Pallenberg, *Inorg. Chem.* 36 (1997) 172-176.
- [21] C. Vogler, H. -D. Hausen, W. Kaim, S. Kohlmann, H. E. A. Kramer, J. Rieker, *Angew. Chem., Int. Ed. Engl.* 28 (1989) 1659-1660.
- [22] V. W. W. Yam, K. K. W. Lo, *J. Chem. Soc., Dalton Trans.* (1995) 499-500.
- [23] S. J. Huang, V. Paneccasio, F. DiBattista, D. Picker, G. Wilson, *J. Org. Chem.* 40 (1975) 124 - 130.
- [24] V. W. -W. Yam, K. K. -W. Lo, W. K. -M. Fung, C. -R. Wang, *Coord. Chem. Rev.* 171 (1998) 17-41.

- [25] M. M. Bagheri-Mohagheghi, N. Shahtahmasebi, M. R. Alinejad, A. Youssefi, M. Shokooh-Saremi, *Physica B* 403 (2008) 2431-2437.
- [26] P. K. Santra, D. Das, T. K. Misra, R. Roy, C. Sinha, S. -M. Peng, *Polyhedron* 18 (1999) 1909-1915.
- [27] S. Goswami, W. Kharmawphlang, A. K. Deb, S. M. Peng, *Polyhedron* 15 (1996) 3635-3641.
- [28] J. Dinda, U. S. Ray, G. Mostafa, T. -H. Lu, A. Usman, I. A. Razak, S. Chantrapromma, H. -K. Fun, C. Sinha, *Polyhedron* 22 (2003) 247-255.
- [29] C. E. Moore, *Natl. Stand. Ref. Data Ser. (US Natl. Bur. Stand.) NSRDS-NBS*, 35 (1971) 116 - 120.
- [30] A. P. de Silva, H. Q. N. Gunaratante, T. Gunnlaugsson, A. J. M. Huxley, C. P. Mc Coy, J. T. Rademacher, T. E. Rice, *Chem. Rev.* 97 (1997) 1515-1566.
- [31] A. K. Satpati, S. Senthilkumar, M. Kumbhakar, S. Nath, D. K. Maity, H. Pal, *Photochem. Photobiol.* 81 (2005) 270-278.
- [32] C. Coenjarts, O. Garcia, L. Llauger, A. L. Vinette, J. C. Scaiano, J. C. Mapping, *J. Am. Chem. Soc.* 125 (2003) 620-621.
- [33] J. C. Scaiano, C. Aliaga, M. N. Chretien, M. Frenette, K. S. Focsaneanu, L. Mikelson, *Pure Appl. Chem.* 77 (2005) 1009-1018.
- [34] M. L. Viriota, M. C. Carre, C. Geoffroy-Chapotot, A. Brembilla, S. Muller, J. F. Stoltz, *Clin. Hemorheol. Microcirculation* 19 (1998) 151-160.
- [35] E. Binetti, A. Panniello, L. Triggiani, R. Tommasi, A. Agostiano, M. L. Curri, M.

- Striccoli, *J Phys Chem B* 116 (2012) 3512-3518.
- [36] J. L. Klappa, A. A. Geers, S. J. Schmidtke, L. A. MacManus-Spencer, K. McNeill, *Dalton Trans.* (2004) 883-891.
- [37] K. Chen, Y. -M. Cheng, Y. Chi, M. -L. Ho, C. -H. Lai, P. -T. Chou, S. -M. Peng, G. -H. Lee, *Chem.—An Asian J.* 2 (2007) 155-163.
- [38] O. Horvath, S. Papp, *J. Photochem.* 30 (1985) 47-61.
- [39] A. L-Cambot, Martine Cantuel, Yoann Leydet, G. Jonusauskasb, D. M. Bassania, N. D. McClenaghan, *Coord. Chem. Rev.* 252 (2008) 2572–2584.
- [40] H. Wang, P. Zhao, D. Shao, J. Zhang, Y. Zhu, *Struct. Chem.* 20 (2009) 995-1003.
- [41] G. Ambrosi, S. Ciattini, M. Formica, V. F. L. Giorgi, E. Macedi, M. Micheloni, P. Paoli, P. Rossi, G. Zappia, *Chem. Commun.* (2009) 7039-7041.
- [42] T. K. Misra, D. Das and C. Sinha, *Polyhedron* 16 (1997) 4163 - 4170.
- [43] D. Datta and A. Chakravorty, *Inorg. Chem.*, 22 (1983) 1085-1090.
- [44] P. K. Santra, D. Das ,T. K. Misra, R. Roy, C. Sinha and S. -M. Peng, *Polyhedron*, 18 (1999) 1909-1915.
- [45] S. Roy, P. Gayen, R. Saha, T. K. Mondal, C. Sinha, *Inorg. Chim. Acta* 410 (2014) 202–213.
- [46] F. Ahmed, J. Datta, B. Dutta, K. Naskar, C. Sinha, S. M. Alam, S. Kundu, P. P. Ray, M. H. Mir, *RSC Advances*, 7 (2017) 10369-10375.
- [47] K. Naskar, A. Dey, B. Dutta, F. Ahmed, C. Sen, M H Mir, P P Roy and C.Sinha, *Cryst. Growth Des.* (2017), DOI: 10.1021/acs.cgd.7b00251.

- [48] G. Matsubayashi, T. Maikawa, H. Tamura, M. Nakano and R. Arakawa, *J. Chem. Soc., Dalton Trans.* (1996) 1539-1544.
- [49] E. D. Glowacki, M. Irimia-Vladu, S. Bauer and N. S. Sariciftcia, *J. Mater. Chem. B*, 1 (2013) 3742–3753
- [50] A. I. Vogel, *A Text Book of Practical Organic Chemistry*, Longmann, London (1959).
- [51] G. A. Crosby, J. N. Demas, *J. Phys. Chem.* 75 (1971) 991-1024.
- [52] D. V. O'Connor, D. Phillips, *Time Correlated Single Photon Counting*, Academic Press, New York (1984).
- [53] B. Valuer, *Molecular Fluorescence: Principles and Applications*, Wiley-VCH, Weinheim (2001).
- [54] J. Tauc, R. Grigorovici, A. Vancu, *Phys. Status Solidi*, 15 (1966) 627-637.
- [55] Program name. Bruker AXS Inc., Madison, Wisconsin, USA (2001).
- [56] G. M. Sheldrick, *SHELXS97*, Program for the solution of crystal structure, University of Göttingen, Germany (1997).
- [57] G. M. Sheldrick, *SHELXL97*, Program for crystal structure refinement, University of Göttingen, Germany (1997).
- [58] A.L. Spek, *J. Appl. Crystallogr.* 36 (2003) 7-13.
- [59] C. Lee, W. Yang, R. G. Parr, *Phys. Rev. B*, 37 (1988) 785-789.
- [60] Gaussian 03, Revision D.01, M. J. Frisch, G. W. Trucks, H. B. Schlegel, G. E. Scuseria,

M. A. Robb, J. R. Cheeseman, J. A. Jr. Montgomery, T. Vreven, K. N. Kudin, J. C. Burant, J. M. Millam, S. S. Iyengar, J. Tomasi, V. Barone, B. Mennucci, M. Cossi, G. Scalmani, N. Rega, G. A. Petersson, H. Nakatsuji, M. Hada, M. Ehara, K. Toyota, R. Fukuda, J. Hasegawa, M. Ishida, T. Nakajima, Y. Honda, O. Kitao, H. Nakai, M. Klene, X. Li, J. E. Knox, H. P. Hratchian, J. B. Cross, V. Bakken, C. Adamo, J. Jaramillo, R. Gomperts, R. E. Stratmann, O. Yazyev, A. J. Austin, R. Cammi, C. Pomelli, J. W. Ochterski, P. Y. Ayala, K. Morokuma, G. A. Voth, P. Salvador, J. J. Dannenberg, V. G. Zakrzewski, S. Dapprich, A. D. Daniels, M. C. Strain, O. Farkas, D. K. Malick, A. D. Rabuck, K. Raghavachari, J. B. Foresman, J. V. Ortiz, Q. Cui, A. G. Baboul, S. Clifford, J. Cioslowski, B. B. Stefanov, G. Liu, A. Liashenko, P. Piskorz, I. Komaromi, R. L. Martin, D. J. Fox, T. Keith, M. A. Al-Laham, C. Y. Peng, A. Nanayakkara, M. Challacombe, P. M. W. Gill, B. Johnson, W. Chen, M. W. Wong, C. Gonzalez, J. A. Pople, *Gaussian Inc.*, Wallingford CT, 2004.

[61] GaussView3.0, Gaussian: Pittsburgh, PA.

[62] P.J. Hay, W. R. Wadt, *J. Chem. Phys.* 82 (1985) 270-283.

[63] N. M. O'Boyle, A. L. Tenderholt, K. M. Langner, *J. Comput. Chem.* 29 (2008) 839-845.

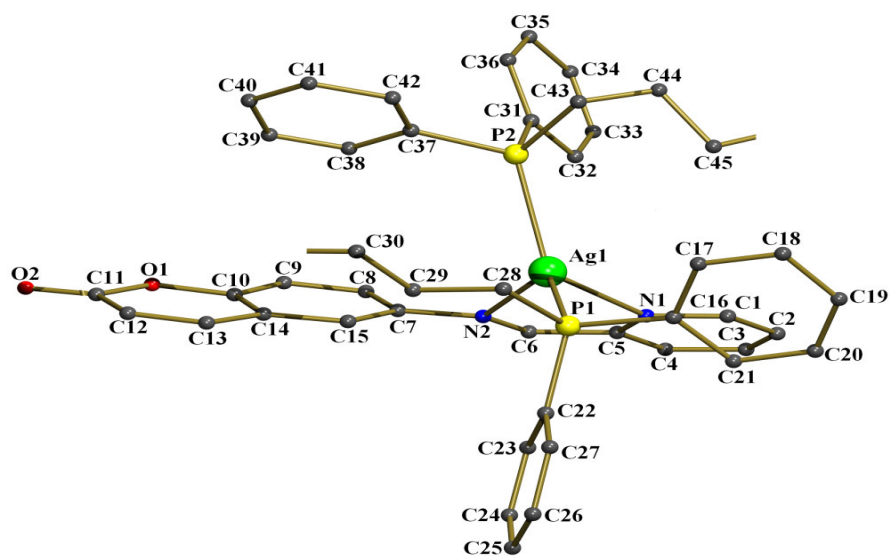


Fig. 1. The molecular structure of $1/n [-Ag(L)(\mu-dpph)^-]_n$ ($6a^+$)

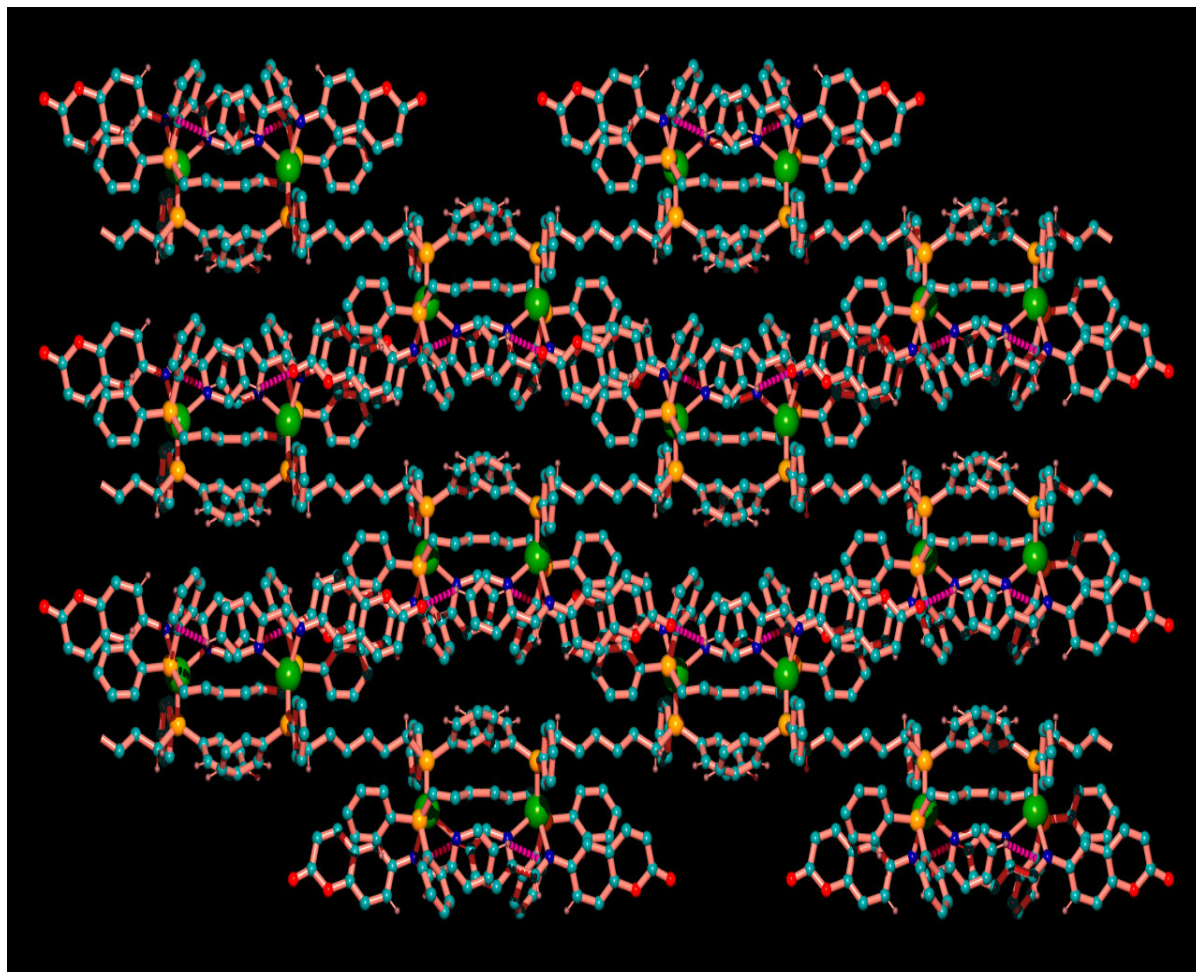


Fig. 2. 3D supramolecular structure of $[-\text{Ag}(\text{L})(\mu\text{-dpph})\text{-}]_n (\text{NO}_3)_n$ (**6a**)

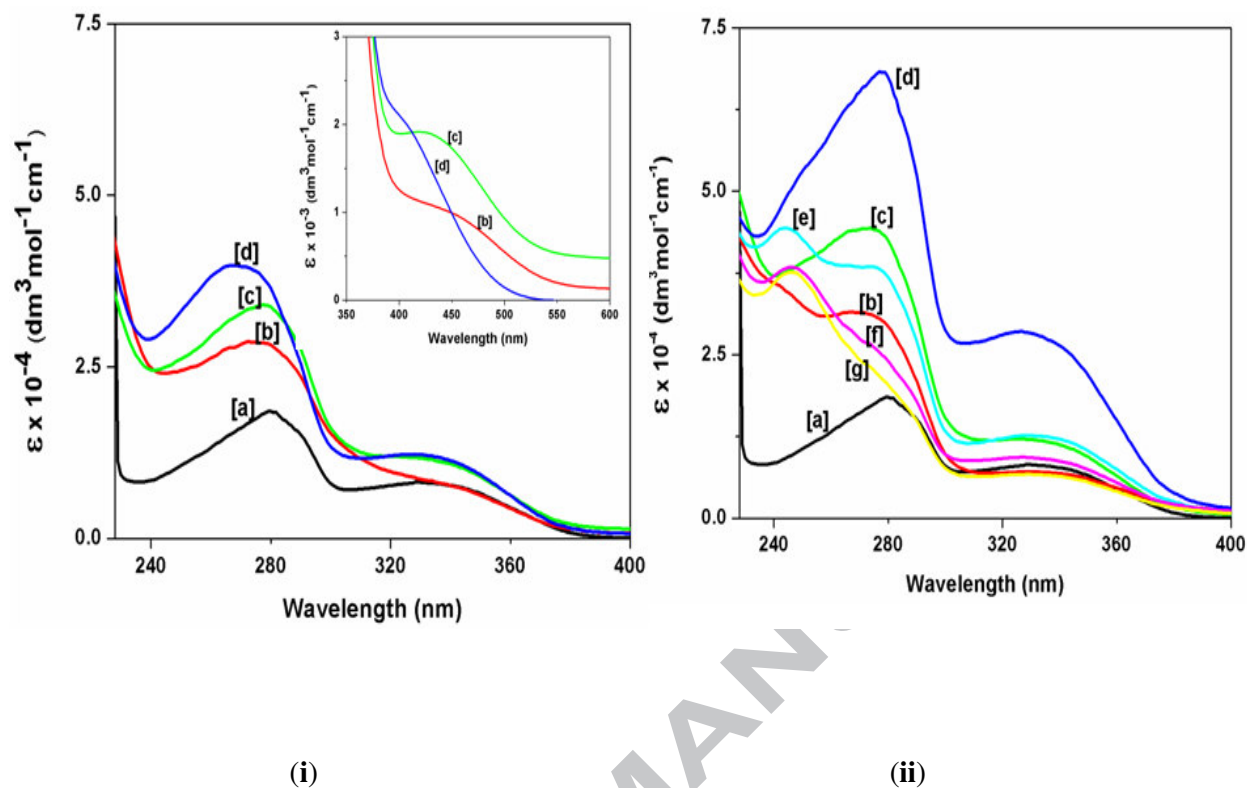


Fig. 3. (i) Absorption spectra of [a] L, [b] $[-\text{Cu}(\text{L})(\mu\text{-dppp})\text{-}]_n(\text{ClO}_4)_n$ (**1**); [c] $[-\text{Cu}(\text{L})(\mu\text{-dppb})\text{-}]_n(\text{ClO}_4)_n$ (**3**), [d] $[-\text{Cu}(\text{L})(\mu\text{-dpph})\text{-}]_n(\text{ClO}_4)_n$ (**5**) (Inset figure at higher concentration), (ii) : [a] L, [b] $[-\text{Ag}(\text{L})(\mu\text{-dppp})\text{-}]_n(\text{NO}_3)_n$ (**2a**), [c] $[-\text{Ag}(\text{L})(\mu\text{-dppp})\text{-}]_n(\text{ClO}_4)_n$ (**2b**), [d] $[-\text{Ag}(\text{L})(\mu\text{-dppb})\text{-}]_n(\text{NO}_3)_n$ (**4a**), [e] $[-\text{Ag}(\text{L})(\mu\text{-dppb})\text{-}]_n(\text{ClO}_4)_n$ (**4b**), [f] $[-\text{Ag}(\text{L})(\mu\text{-dpph})\text{-}]_n(\text{NO}_3)_n$ (**6a**), [g] $[-\text{Ag}(\text{L})(\mu\text{-dpph})\text{-}]_n(\text{ClO}_4)_n$ (**6b**) in CH_3CN

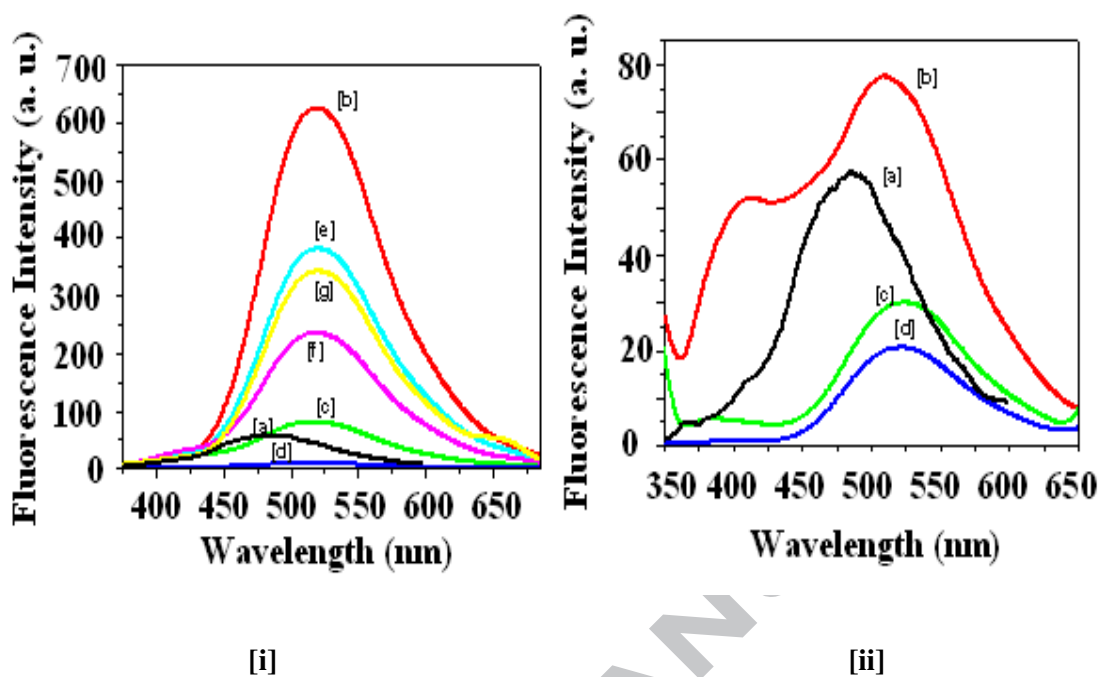


Fig. 4. Fluorescence spectra (irradiation λ , nm): [i] [a] L, [b] $[-\text{Cu}(\text{L})(\mu\text{-dppp})\text{-}]_n(\text{ClO}_4)_n$ (**1**) (338 nm); [c] $[-\text{Cu}(\text{L})(\mu\text{-dppb})\text{-}]_n(\text{ClO}_4)_n$ (**3**) (333 nm), [d] $[-\text{Cu}(\text{L})(\mu\text{-dpph})\text{-}]_n(\text{ClO}_4)_n$ (**5**) (330 nm), [ii]: [a] L, [b] $[-\text{Ag}(\text{L})(\mu\text{-dppp})\text{-}]_n(\text{NO}_3)_n$ (**2a**) (336 nm), [c] $[-\text{Ag}(\text{L})(\mu\text{-dppp})\text{-}]_n(\text{ClO}_4)_n$ (**2b**) (332 nm), [d] $[-\text{Ag}(\text{L})(\mu\text{-dppb})\text{-}]_n(\text{NO}_3)_n$ (**4a**) (329 nm), [e] $[-\text{Ag}(\text{L})(\mu\text{-dppb})\text{-}]_n(\text{ClO}_4)_n$ (**4b**) (333 nm), [f] $[-\text{Ag}(\text{L})(\mu\text{-dpph})\text{-}]_n(\text{NO}_3)_n$ (**6a**) (334 nm), [g] $[-\text{Ag}(\text{L})(\mu\text{-dpph})\text{-}]_n(\text{ClO}_4)_n$ (**6b**) (333 nm) in CH_3CN

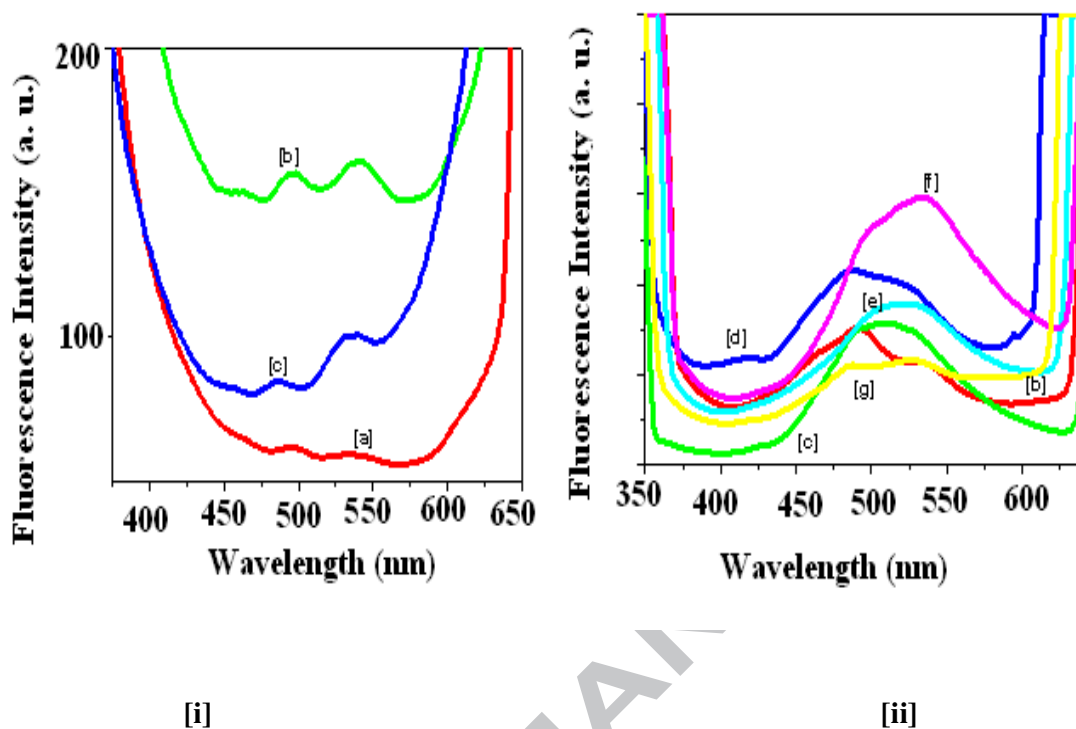


Fig. 5. Fluorescence spectra of [i] [a] $[-\text{Cu}(\text{L})(\mu\text{-dppp})\text{-}]_n(\text{ClO}_4)_n$ (**1**); [b] $[-\text{Cu}(\text{L})(\mu\text{-dppb})\text{-}]_n(\text{ClO}_4)_n$ (**3**), [c] $[-\text{Cu}(\text{L})(\mu\text{-dpph})\text{-}]_n(\text{ClO}_4)_n$ (**5**); [ii] [b] $[-\text{Ag}(\text{L})(\mu\text{-dppp})\text{-}]_n(\text{NO}_3)_n$ (**2a**), [c] $[-\text{Ag}(\text{L})(\mu\text{-dppp})\text{-}]_n(\text{ClO}_4)_n$ (**2b**), [d] $[-\text{Ag}(\text{L})(\mu\text{-dppb})\text{-}]_n(\text{NO}_3)_n$ (**4a**), [e] $[-\text{Ag}(\text{L})(\mu\text{-dppb})\text{-}]_n(\text{ClO}_4)_n$ (**4b**), [f] $[-\text{Ag}(\text{L})(\mu\text{-dpph})\text{-}]_n(\text{NO}_3)_n$ (**6a**), and [g] $[-\text{Ag}(\text{L})(\mu\text{-dpph})\text{-}]_n(\text{ClO}_4)_n$ (**6b**) in solid state

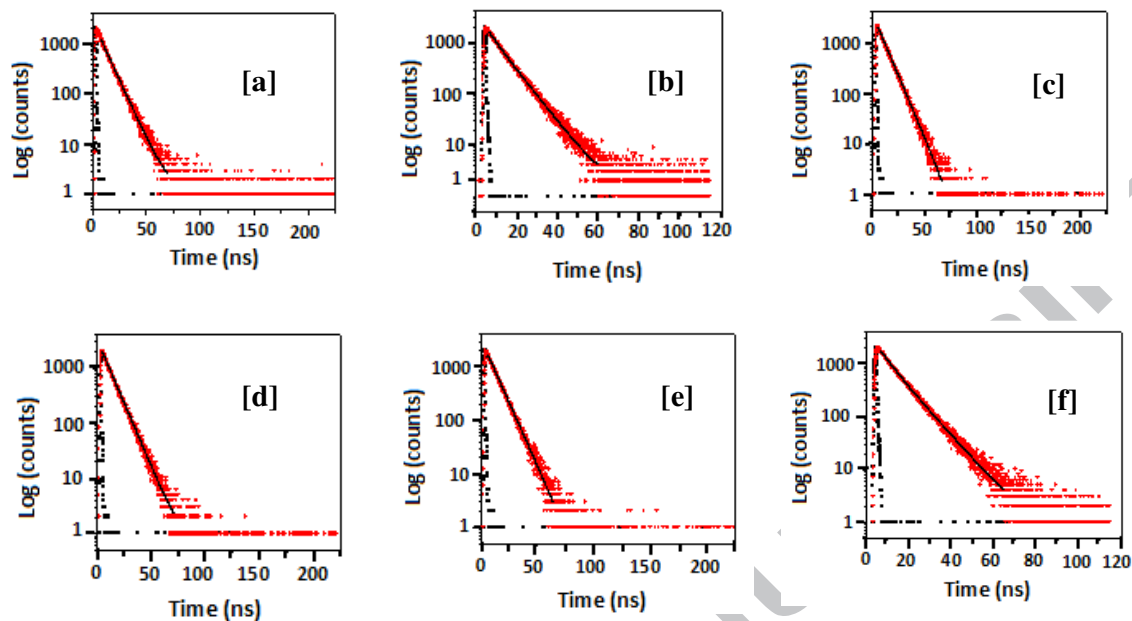


Fig. 6. Exponential decay profile (●) and fitting curve (—) of [a] $[-\text{Cu}(\text{L})(\mu\text{-dppp})\text{-}]_n(\text{ClO}_4)_n$ (**1**), [b] $[-\text{Cu}(\text{L})(\mu\text{-dpph})\text{-}]_n(\text{ClO}_4)_n$ (**5**), [c] $[-\text{Ag}(\text{L})(\mu\text{-dppp})\text{-}]_n(\text{NO}_3)_n$ (**2a**), [d] $[-\text{Ag}(\text{L})(\mu\text{-dpph})\text{-}]_n(\text{NO}_3)_n$ (**6a**), [e] $[-\text{Ag}(\text{L})(\mu\text{-dppp})\text{-}]_n(\text{ClO}_4)_n$ (**2b**) and [f] $[-\text{Ag}(\text{L})(\mu\text{-dpph})\text{-}]_n(\text{ClO}_4)_n$ (**6b**) in CH_3CN . Excitation is carried out at 370 nm.

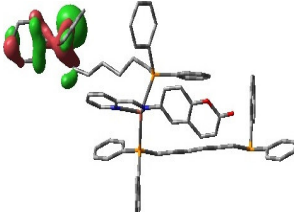
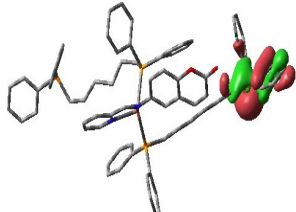
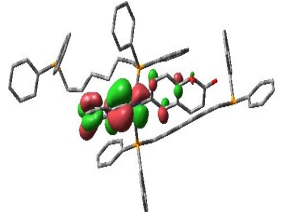
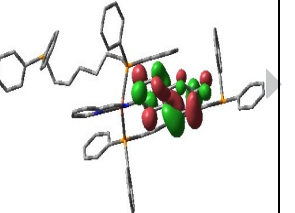
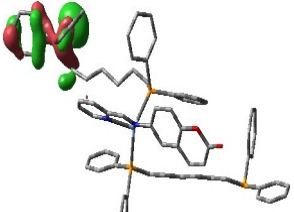
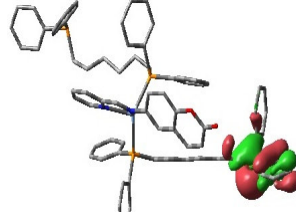
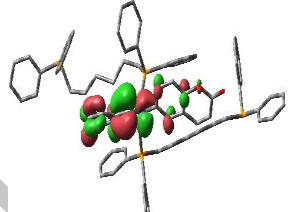
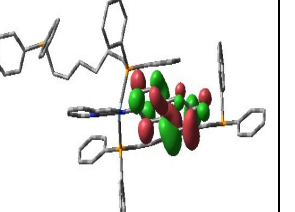
[Cu(L)(μ-dpph)]⁺			
			
HOMO-1, -7.11 eV; dpph, 100 %.	HOMO, -6.81 eV; dpph, 100 %.	LUMO, -4.79 eV; L, 97 %.	LUMO+1, -4.07 eV; L, 98 %.
[Ag(L)(μ-dpph)]⁺			
			
HOMO-1, -7.12 eV; dpph, 100 %.	HOMO, -6.76 eV; dpph, 100 %.	LUMO, -4.92 eV; L, 97%.	LUMO+1, -4.08 eV; L, 99%.

Fig. 7. Contour plots of some selected MOs of [Cu(L)(μ -dpph)]⁺ and [Ag(L)(μ -dpph)]⁺

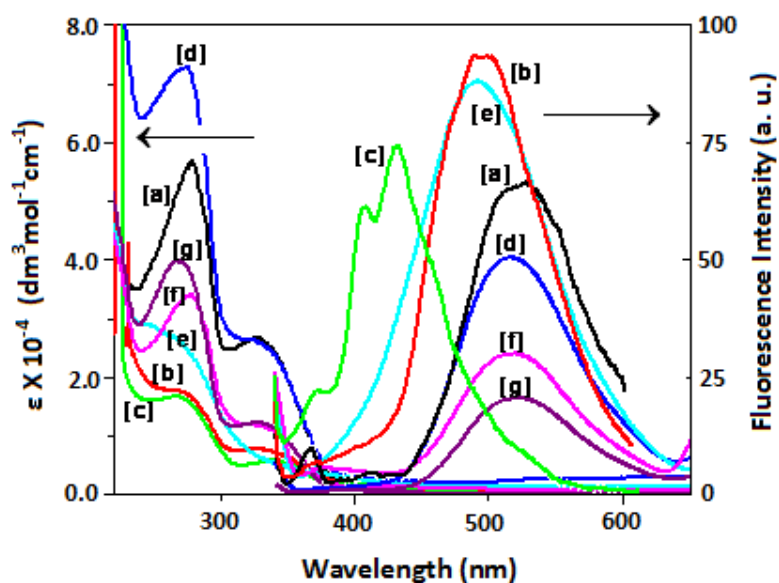


Fig. 8. Absorption and emission spectra of [a] $[\text{Cu}(\text{L})_2]\text{ClO}_4$, [b] $[\text{CuCl}(\text{L})(\text{PPh}_3)]$, [c] $[\text{Cu}(\text{L})(\text{PPh}_3)_2]\text{ClO}_4$, [d] $[(\text{L})\text{Cu}(\mu\text{-dppm})_2\text{Cu}(\text{L})](\text{ClO}_4)_2$ (**1**) (338 nm), [e] $[(\text{L})(\text{CH}_3\text{CN})\text{Cu}(\mu\text{-dppe})\text{Cu}(\text{L})(\text{CH}_3\text{CN})](\text{ClO}_4)_2$, [f] $[-\text{Cu}(\text{L})(\mu\text{-dppb})-]_n(\text{ClO}_4)_n$ and [g] $[-\text{Cu}(\text{L})(\mu\text{-dpph})-]_n(\text{ClO}_4)_n$ in CH_3CN medium.

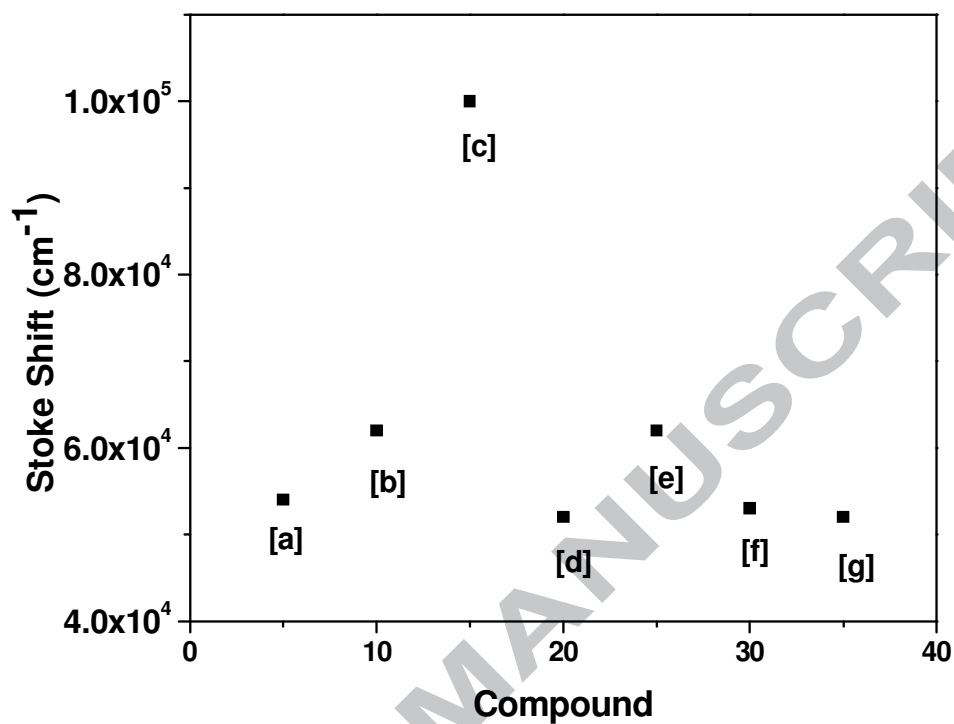


Fig. 9. Comparative Stoke's Shift of [a] $[\text{Cu}(\text{L})_2]\text{ClO}_4$, [b] $[\text{CuCl}(\text{L})(\text{PPh}_3)]$, [c] $[\text{Cu}(\text{L})(\text{PPh}_3)_2]\text{ClO}_4$, [d] $[(\text{L})\text{Cu}(\mu\text{-dppm})_2\text{Cu}(\text{L})](\text{ClO}_4)_2$, [e] $[(\text{L})\text{Cu}(\text{CH}_3\text{CN})(\mu\text{-dppe})\text{Cu}(\text{CH}_3\text{CN})(\text{L})](\text{ClO}_4)_2$, [f] $[-\text{Cu}(\text{L})(\mu\text{-dppb})-]_n(\text{ClO}_4)_n$ and [g] $[-\text{Cu}(\text{L})(\mu\text{-dpph})-]_n(\text{ClO}_4)_n$ in CH_3CN medium.

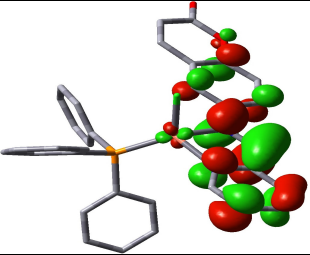
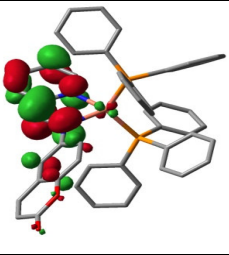
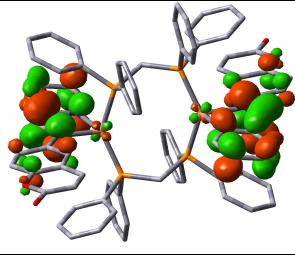
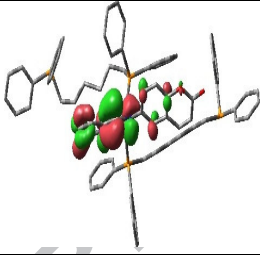
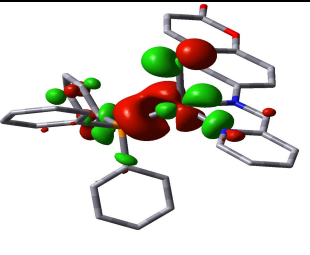
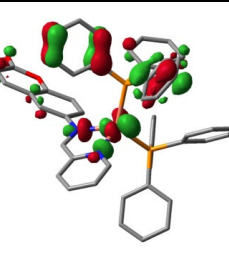
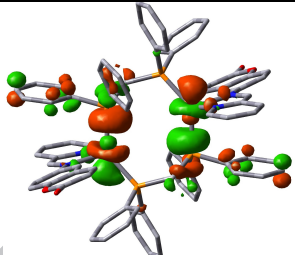
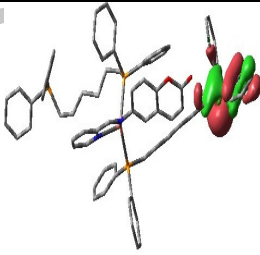
[CuCl(L)(PPh ₃)]	[Cu(L)(PPh ₃) ₂ ClO ₄]	[(L)Cu(μ-dppm) ₂ Cu(L)](ClO ₄) ₂	[Cu(L)(μ-dpph)] ⁺
			
LUMO, -2.86 eV; L, 97; Cu, 02; PPh ₃ , 00; Cl, 01%	LUMO, -5.06 eV; L, 96; Cu, 03; PPh ₃ , 01%	LUMO, -6.87 eV; L, 96; Cu, 02; dppm, 02%	LUMO, -4.79 eV; L, 97; Cu, 01; dpph, 02%
			
HOMO, -5.27 eV; L, 02; Cu, 36; PPh ₃ , 15; Cl, 47%	HOMO, -8.14 eV; L, 5; Cu, 31; PPh ₃ , 64%	HOMO, -10.11 eV; L, 07; Cu, 46; dppm, 47%	HOMO, -6.81 eV; L, 00; Cu, 00; dpph, 100%
HOMO-LUMO Energy Difference (eV)			
2.41 eV	3.08 eV	3.24 eV	2.02 eV

Fig. 10. Contour plots of some selected MOs of [CuCl(L)(PPh₃)], [Cu(L)(PPh₃)₂ClO₄], [(L)Cu(μ-dppm)₂Cu(L)](ClO₄)₂ and 1/n [Cu(L)(μ-dpph)]_n⁺

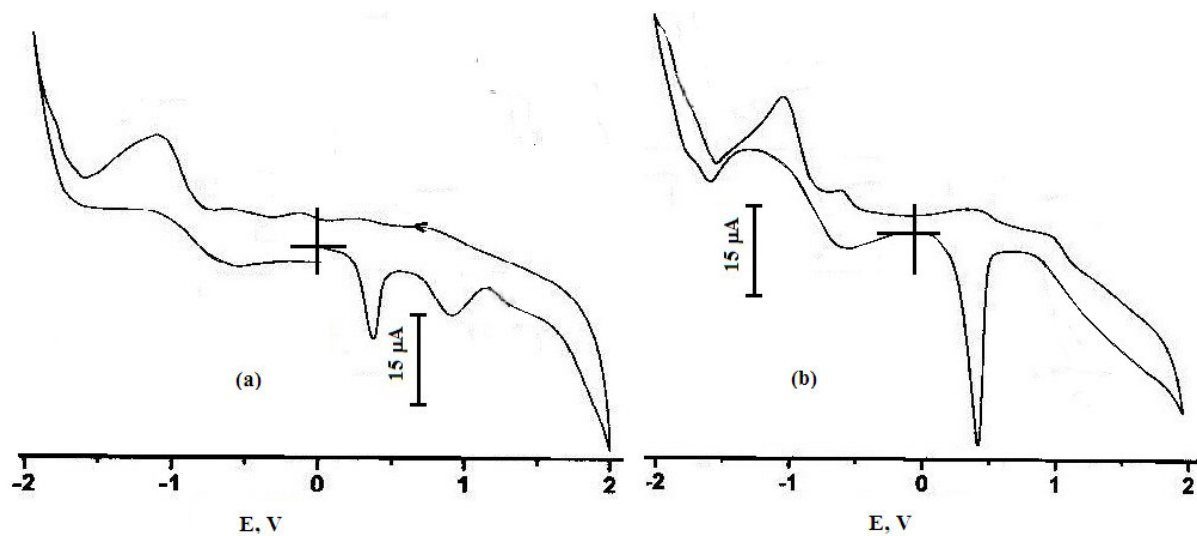


Fig. 11. Representative Cyclic voltammogram of (a) [-Cu(L)(μ-dppp)-]_n(ClO₄)_n (**1**) and (b) [-Ag(L)(μ-dppp)-]_n(ClO₄)_n (**2b**) in MeCN solution using Pt-disk working electrode, Ag/AgCl, Cl⁻ (reference electrode) and Pt-wire (Auxiliary electrode) with [n-Bu₄N]ClO₄ as supporting electrolyte

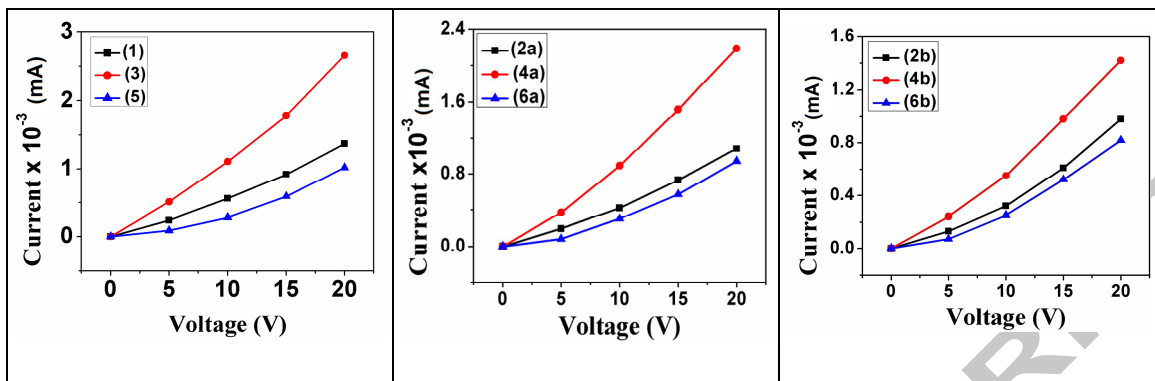


Fig. 12. Current-Voltage characteristic curves of the complexes : $[-\text{Cu}(\text{L})(\mu\text{-dppp})\text{-}]_n(\text{ClO}_4)_n$ (1); $[-\text{Cu}(\text{L})(\mu\text{-dppb})\text{-}]_n(\text{ClO}_4)_n$ (3), $[-\text{Cu}(\text{L})(\mu\text{-dpph})\text{-}]_n(\text{ClO}_4)_n$ (5), $[-\text{Ag}(\text{L})(\mu\text{-dppp})\text{-}]_n(\text{NO}_3)_n$ (2a), $[-\text{Ag}(\text{L})(\mu\text{-dppb})\text{-}]_n(\text{NO}_3)_n$ (4a), $[-\text{Ag}(\text{L})(\mu\text{-dpph})\text{-}]_n(\text{NO}_3)_n$ (6a), $[-\text{Ag}(\text{L})(\mu\text{-dppp})\text{-}]_n(\text{ClO}_4)_n$ (2b), $[-\text{Ag}(\text{L})(\mu\text{-dppb})\text{-}]_n(\text{ClO}_4)_n$ (4b), $[-\text{Ag}(\text{L})(\mu\text{-dpph})\text{-}]_n(\text{ClO}_4)_n$ (6b)

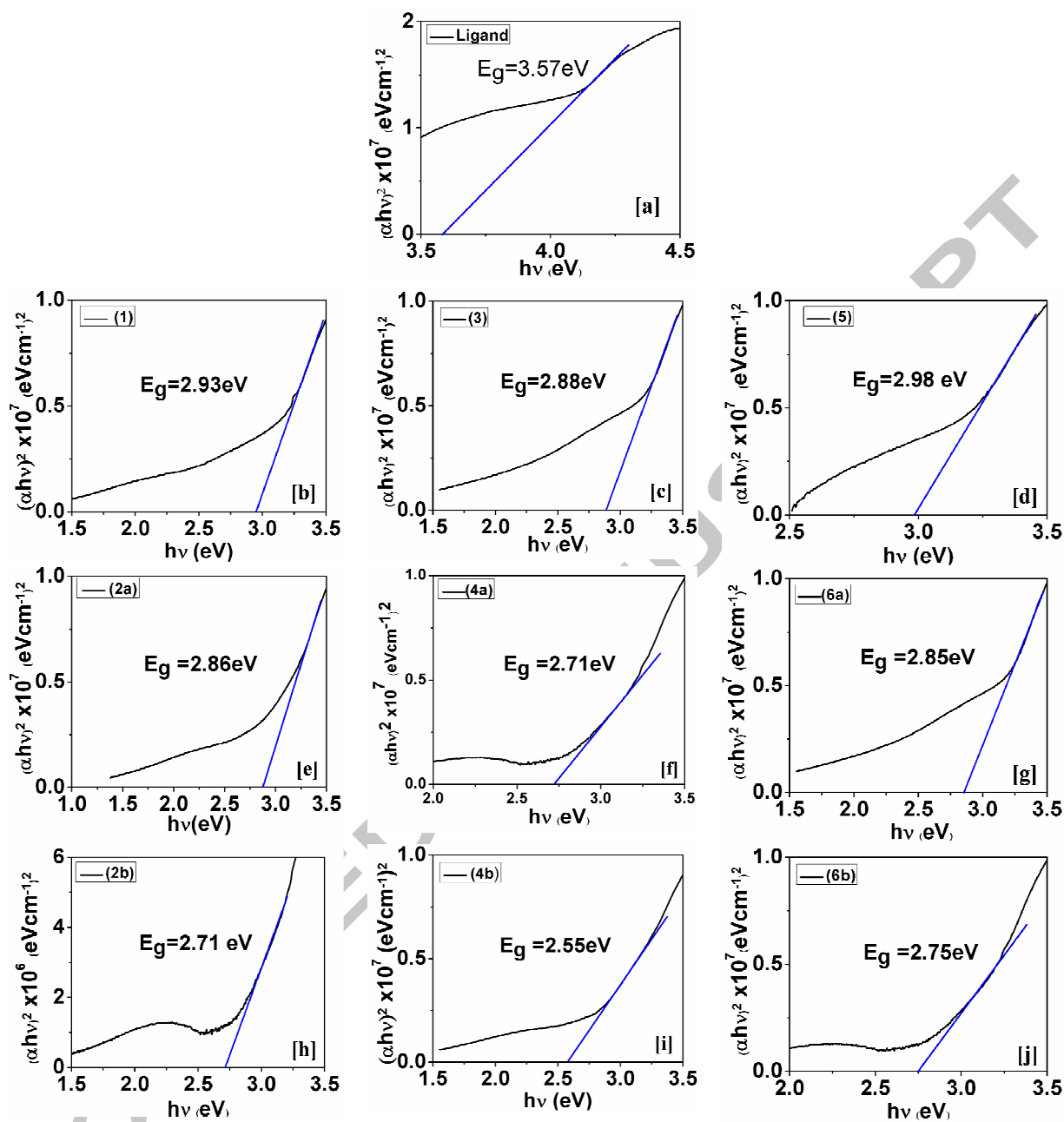


Fig. 13. Tauc's plots for Band Gap measurement of [a] [L], [b] [-Cu(L)(μ -dppp)-]_n(ClO₄)_n (1); [c] [-Cu(L)(μ -dppb)-]_n(ClO₄)_n (3), [d] [-Cu(L)(μ -dpph)-]_n(ClO₄)_n (5), [e] [-Ag(L)(μ -dppp)-]_n(NO₃)_n (2a), [f] [-Ag(L)(μ -dppb)-]_n(NO₃)_n (4a), [g] [-Ag(L)(μ -dpph)-]_n(NO₃)_n (6a), [h] [-Ag(L)(μ -dppp)-]_n(ClO₄)_n (2b), [i] [-Ag(L)(μ -dppb)-]_n(ClO₄)_n (4b), [j] [-Ag(L)(μ -dpph)-]_n(ClO₄)_n (6b)

Table 1. Selected bond lengths and bond angles of $[-\text{Ag}(\text{L})(\mu\text{-dpph})\text{-}]_n(\text{NO}_3)_n$ (**6a**)

Bond lengths (Å)		Bond angles (°)	
Ag(1)–N(1)	2.412(5)	N(2)–Ag(1)–N(1)	69.29(16)
Ag(1)–N(2)	2.384(4)	N(2)–Ag(1)–P(1)	126.52(11)
Ag(1)–P(1)	2.4170(15)	N(2)–Ag(1)–P(2)	102.20(11)
Ag(1)–P(2)	2.4768(16)	P(1)–Ag(1)–N(1)	107.06(13)
N(1)–C(1)	1.353(7)	N(1)–Ag(1)–P(2)	117.03(13)
N(1)–C(5)	1.317(7)	P(1)–Ag(1)–P(2)	123.26(5)
N(2)–C(6)	1.274(6)	C(5)–N(1)–Ag(1)	115.0(3)
N(2)–C(7)	1.433(6)	C(6)–N(2)–Ag(1)	116.6(4)

Table 2. UV-Vis, Fluorescence, Lifetime[†] and Cyclic voltammetric data of copper(I) and silver(I) complexes

Compound	Fluorescence Data [*]				Fluorescence Decay Data [†]				Cyclic voltammogram	
	λ_{ex} (nm)	λ_{em} (nm)	λ'_{em} (nm)	Φ	χ^2	τ (ns)	$k_r \times 10^{-9}$	$k_{nr} \times 10^{-9}$	E(V) (ΔE_p , mV)	
									E_M	E_L
[-Cu(L)(μ -dppp)Cu(L)-] _n (ClO ₄) _{2n} (1)	338	411, 509	462, 494, 534	0.046	1.17	9.28	0.0050	0.1028	0.33, 0.89	-0.66(140), -1.13
[-Ag(L)(μ -dppp)Ag(L)-] _n (NO ₃) _{2n} (2a)	336	519	462, 491, 535	0.102	0.98	8.96	0.0114	0.1002	0.41	-0.60(40), -1.02
[-Ag(L)(μ -dppp)Ag(L)-] _n (ClO ₄) _{2n} (2b)	332	515	511, 531	0.089	1.18	9.16	0.0009	0.1083	0.36	-0.64(70), -0.92
[-Cu(L)(μ -dppb)Cu(L)-] _n (ClO ₄) _{2n} (3)	333	522	463, 497, 540	0.029	1.05	7.44	0.0013	0.1331	0.40, .96	-0.69(150), -1.23
[-Ag(L)(μ -dppb)Ag(L)-] _n (NO ₃) _{2n} (4a)	329	516	414, 485, 528	0.059	1.25	9.20	0.0006	0.1081	0.50	-0.59(120), -0.97
[-Ag(L)(μ -dppb)Ag(L)-] _n (ClO ₄) _{2n} (4b)	333	519	460, 522	0.045	0.98	7.50	0.0059	0.1274	0.43	-0.62(150), -1.38
[-Cu(L)(μ -dpph)Cu(L)-] _n (ClO ₄) _{2n} (5)	330	521	457, 485, 537	0.017	1.06	7.91	0.0001	0.1263	0.38, 0.97	-0.63(130), -1.12
[-Ag(L)(μ -dpph)Ag(L)-] _n (NO ₃) _{2n} (6a)	334	518	498, 535	0.035	1.02	9.43	0.0037	0.1023	0.33	-0.62(70), -0.98
[-Ag(L)(μ -dpph)Ag(L)-] _n (ClO ₄) _{2n} (6b)	333	519	459, 486, 531	0.021	0.99	8.54	0.0024	0.1148	0.42	-0.65(130), -1.36

[†]Solvent, MeCN, Pt-working electrode, Ag/AgCl reference Electrode, Pt-auxiliary electrode; [n-Bu₄N](ClO₄) supporting electrolyte, scan rate 100 mV/sec; metal oxidation $E_M = 0.5 (E_{pa} + E_{pc})$, V, $\Delta E_p = |E_{pa} - E_{pc}|$, mV; E_L refers to ligand reduction. ^{*} λ_{ex} (nm) and λ_{em} (nm) in solution phase and λ'_{em} (nm) in solid phase. [†] Free ligand lifetime 0.92 ns [Ref. 15].

Table 3. I/V plot and energy band gap data of all the polymeric complexes

Complex	Energy	*Electrical Conductivity(σ)
	Band Gap (eV)	($S m^{-1}$)
$[-Cu(L)(\mu-dppp)]_n(ClO_4)_n$ (1)	2.93	2.71×10^{-3}
$[-Ag(L)(\mu-dppp)]_n(NO_3)_n$ (2a)	2.86	1.92×10^{-3}
$[-Ag(L)(\mu-dppp)]_n(ClO_4)_n$ (2b)	2.71	2.92×10^{-3}
$[-Cu(L)(\mu-dppb)]_n(ClO_4)_n$ (3)	2.88	4.38×10^{-3}
$[-Ag(L)(\mu-dppb)]_n(NO_3)_n$ (4a)	2.71	4.17×10^{-3}
$[-Ag(L)(\mu-dppb)]_n(ClO_4)_n$ (4b)	2.55	4.35×10^{-3}
$[-Cu(L)(\mu-dpph)]_n(ClO_4)_n$ (5)	2.98	1.95×10^{-3}
$[-Ag(L)(\mu-dpph)]_n(NO_3)_n$ (6a)	2.85	2.00×10^{-3}
$[-Ag(L)(\mu-dpph)]_n(ClO_4)_n$ (6b)	2.75	1.46×10^{-3}

Table 4. Crystallographic parameters of [-Ag(L)(μ -dpph)-]_n(NO₃)_n (**6a**)

Empirical formula	C ₄₅ H ₄₂ Ag N ₂ O ₂ P ₂ , N O ₃
Formula weight	874.63
Crystal system	Monoclinic
Space group	C2/c (No. 15)
a (Å)	12.4796(12)
b (Å)	22.354(3)
c (Å)	31.006(3)
α (°)	90.00
β (°)	96.757(2)
γ (°)	90.00
V(Å ³)	8589.6(16)
Z	8
ρ (calculated) (g cm ⁻³)	1.353
Absorption coefficient (mm ⁻¹)	0.591
F(000)	3600
T(K)	293
Total reflection collected	43984
Uniq. Data	8552
R(int)	0.066
Observed data [I > 2.0 σ (I)]	4893
Nref	8552
Npar	499
R	0.0607
wR2	0.2130
S	0.94
Max. and Av. Shift/Error	0.01, 0.00
Min. and Max. Resd. Dens. [e/Ång ³]	-0.64, 1.48

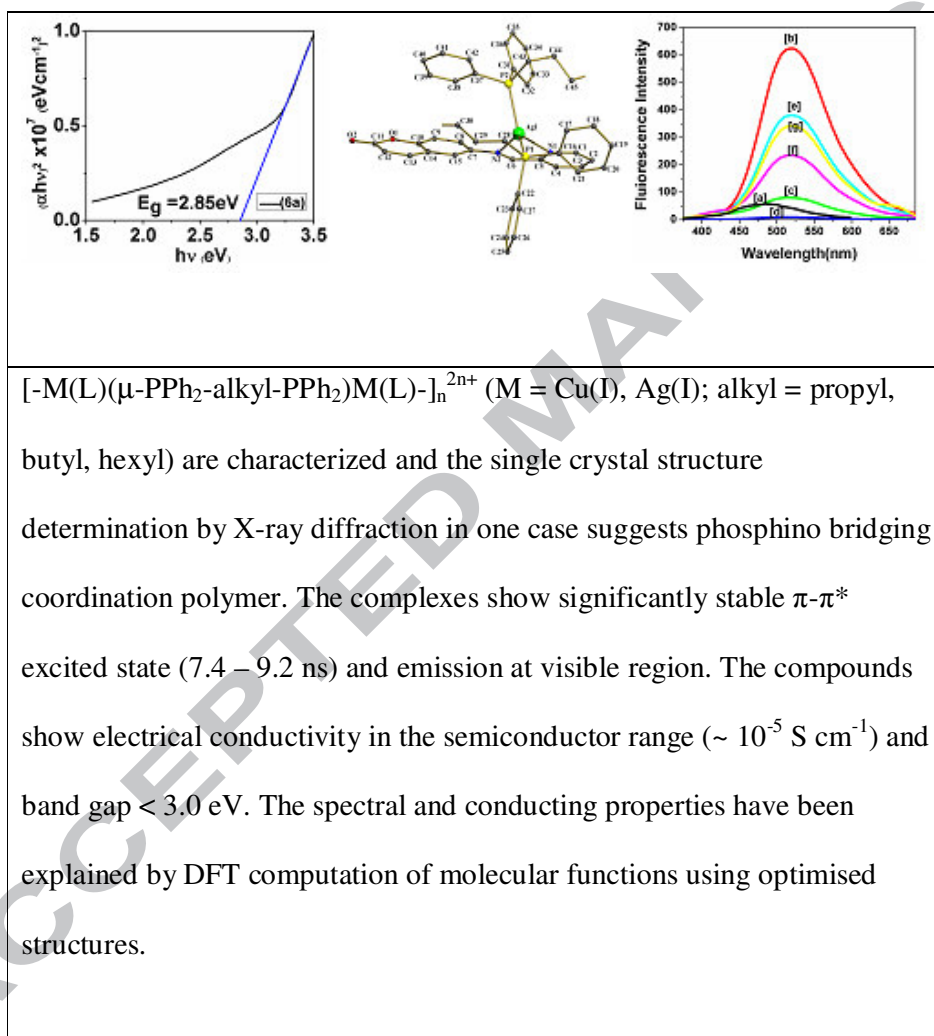
$${}^a R = \sum ||F_o| - |F_c|| / \sum |F_o|, \quad {}^b wR = \{ \sum [w(F_o^2 - F_c^2)^2] / \sum [w(F_o^2)^2] \}^{1/2}; \quad w = [\sigma^2(F_o)^2 + (0.1373P)^2 +$$

$$0.0091P]^{-1}, \quad \text{where } P = (F_o^2 + 2F_c^2)/3; \quad {}^c \text{Goodness-of-fit}$$

GRAPHICAL ABSTRACT

Structure, spectra and electrical conductivity of Copper(I) and Silver(I) phosphino bridging mixed ligand complexes with Coumarinyl Schiff base

Suman Roy, Tapan Kumar Mondal, Animesh Layek, Rajat Saha, and Chittaranjan Sinha*



HIGHLIGHTS

Structure, spectra and electrical conductivity of Copper(I) and Silver(I) phosphino bridging mixed ligand complexes with Coumarinyl Schiff base

Suman Roy, Tapan Kumar Mondal, Animesh Layek, Rajat Saha, and Chittaranjan Sinha*

- ◆ Copper(I) and Silver(I) complexes of N-{(2-pyridyl)methylidene}-6-coumarin
- ◆ Bridging bis(diphenylphosphino)alkane
- ◆ Structure, spectra, photophysical and redox data
- ◆ Electrical conductivity of polymer and semiconducting band gap
- ◆ DFT computation to explain spectra and redox properties